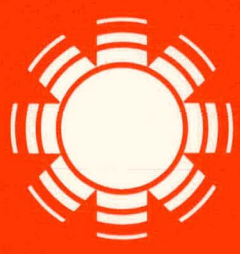SERI/TR-34-093

April 1980

MASTER

Effect of Circumsolar Radiation on Performance of Focusing Collectors

P. Bendt
A. Rabl

SERI

Solar Energy Research Institute
A Division of Midwest Research Institute

1617 Cole Boulevard
Golden, Colorado 80401

DISCLAIMER

This report was prepared as an account of work sponsored by an agency of the United States Government. Neither the United States Government nor any agency Thereof, nor any of their employees, makes any warranty, express or implied, or assumes any legal liability or responsibility for the accuracy, completeness, or usefulness of any information, apparatus, product, or process disclosed, or represents that its use would not infringe privately owned rights. Reference herein to any specific commercial product, process, or service by trade name, trademark, manufacturer, or otherwise does not necessarily constitute or imply its endorsement, recommendation, or favoring by the United States Government or any agency thereof. The views and opinions of authors expressed herein do not necessarily state or reflect those of the United States Government or any agency thereof.

DISCLAIMER

Portions of this document may be illegible in electronic image products. Images are produced from the best available original document.

NOTICE

SERI/TR-34-093
UC Category: UC-62

MASTER

EFFECT OF CIRCUMSOLAR RADIATION
ON PERFORMANCE OF FOCUSING COLLECTORS

P. BENDT
A. RABL

APRIL 1980

PREPARED UNDER TASK NO. 3457.33

Solar Energy Research Institute

1536 Cole Boulevard
Golden, Colorado 80401

A Division of Midwest Research Institute

Prepared for the
U.S. Department of Energy
Contract No. EG·77·C·01·4042

THIS PAGE

WAS INTENTIONALLY

LEFT BLANK

PREFACE

Ari Rabl

Approved for:

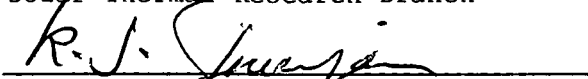SOLAR ENERGY RESEARCH INSTITUTE

Frank Kreith, Branch Chief
Solar Thermal Research Branch

K. J. Touryan, Acting Manager
Solar Thermal, Ocean, and Wind Division

THIS PAGE

WAS INTENTIONALLY

LEFT BLANK

SUMMARY

Circumsolar radiation is one of several factors, along with optical errors (contour, tracking, etc.), that determine the size and shape of the solar image at the receiver of a concentrating collector. The sensitivity of a collector to circumsolar radiation depends on insolation conditions and on collector parameters; it increases with geometrical concentration ratio and decreases with threshold. In this paper the Lawrence Berkeley Laboratory (LBL) circumsolar data are used to calculate the effect of circumsolar radiation on both the instantaneous and the long-term average performance of focusing collectors. To speed up the computations, the optical properties of the concentrator are expressed in terms of an angular acceptance function. The angular acceptance function and the brightness distribution of the sun are then convoluted, a procedure which requires, for each circumsolar scan, only 56 multiplications and additions (one for each of the angular intervals at which the brightness has been measured by the LBL circumsolar telescope). The instantaneous performance corresponding to particular circumsolar scans is of interest for the analysis of test results of collectors with high concentration. For most predictions of long-term average performance a far simpler approach will, however, be adequate. For this purpose a standard synthetic circumsolar scan has been developed that describes the brightness distribution of the solar disk ("limb darkening") and of the circumsolar region. The radiation intercepted by a receiver is calculated once for the solar portion and once for the circumsolar portion of this standard sun shape. The long-term average radiation intercepted by the receiver is then obtained by averaging the solar and the circumsolar intercept factors, weighted according to the long-term average circumsolar ratio for the location and period under study. Tested against hour-by-hour simulations, this simple approach was found to have an rms error of only 0.2%, negligible compared to typical uncertainties in system performance calculations. This analysis points out the usefulness of the long-term average circumsolar ratio as a simple measure of circumsolar radiation.

THIS PAGE

WAS INTENTIONALLY

LEFT BLANK

TABLE OF CONTENTS

THIS PAGE

WAS INTENTIONALLY

LEFT BLANK

SERI ☀

LIST OF FIGURES

THIS PAGE

WAS INTENTIONALLY

LEFT BLANK

LIST OF TABLES

THIS PAGE

WAS INTENTIONALLY

LEFT BLANK

NOMENCLATURE AND DEFINITIONS

$B(\theta)$ angular brightness distribution of sun $(W/m^2$ sterad)

C geometric concentration ratio

$f(\theta)$ angular acceptance function (fraction of parallel beam of radiation incident on aperture that reaches receiver if optics perfect and no absorption losses)

$f_\sigma(\theta)$ smeared angular acceptance function = convolution of $f(\theta)$ with distribution of optical errors (fraction of parallel beam of radiation incident on aperture that reaches receiver if no absorption loss but if optics has Gaussian error distribution of width σ)

F $1 - \gamma_{sc}$

I_b beam irradiance as measured by pyrheliometer at normal incidence (W/m^2)

I_c circumsolar irradiance at normal incidence = radiation coming from the angular range between $\delta = 0.275°$ and $\Delta = 3.2°$ (W/m^2)

I_{in} radiation intercepted by receiver if no absorption losses in optics

I_h hemispherical irradiance on horizontal surface (W/m^2)

I_s irradiance of solar disk at normal incidence (W/m^2)

q_{abs} power per collector aperture area absorbed by collector (W/m^2)

q_{loss} heat loss per aperture area (W/m^2)

q_{out} net power per aperture area delivered by collector (W/m^2)

R $I_c/(I_c + I_s)$ = circumsolar ratio

R_{av} $\overline{I}_c/(\overline{I}_c + \overline{I}_s)$ = long-term average circumsolar ratio

α absorptance of receiver

γ intercept factor with respect to pyrheliometer = I_{in}/I_b

γ_c intercept factor with respect to circumsolar radiation

γ_s intercept factor with respect to radiation from solar disk

γ_{sc} intercept factor with respect to radiation from disk and circumsolar region

η collector efficiency

η_o $(\rho\tau\alpha)\gamma$ = optical efficiency with respect to pyrheliometer

ε relative error between model and data

ρ reflectance

υ rms angular deviation due to optical errors of reflected radiation from design direction

σ_{sun} rms angular width of sun

τ transmittance of collector or receiver glazing

θ angle from center of sun

δ 0.275° = angular radius of sun (within resolution of LBL circumsolar telescope)

Δ 3.2° = angular range of LBL circumsolar telescope

<u>Circumsolar radiation:</u> radiation outside solar disk but within cone of radius $\Delta = 3.2°$

<u>Solar radiation:</u> radiation from solar disk (the solar disk is defined to have angular radius $\delta = 0.275°$ = angular radius of sun within resolution of LBL circumsolar telescope)

<u>Beam radiation:</u> radiation measured by pyrheliometer (also called direct radiation)

<u>Scan (circumsolar):</u> brightness distribution of sun as measured by LBL circumsolar telescope (from $\theta = 0°$ to $\theta = 3.2°$)

<u>Long-term average radiation:</u> average of instantaneous radiation values y_i defined as

$$\overline{y} = \frac{1}{N} \sum_{i=1}^{N} {}^+ y_i$$

averaged over a large number N of data points. The plus sign next to the summation sign indicates that only those data are to be included that are above a specified threshold q.

Whereas the bar notation designates true averages and, in this paper, is used only for radiation values, a different kind of averaging procedure is used for circumsolar ratios and for intercept factors. The latter quantities, denoted by a subscript "av," are ratios of average radiation values.

<u>NIP:</u> normal incidence pyrheliometer

SECTION 1.0

INTRODUCTION

Due to atmospheric scattering, a significant amount of solar radiation arrives at the earth's surface from directions other than the sun. The radiation within a few degrees of the solar disk (the solar aureole) is called circumsolar radiation. Circumsolar radiation poses a problem for the analysis of concentrating collectors because, in general, the acceptance angle or field of view of a concentrator will differ markedly from that of the standard instruments available for measuring the direct or beam component I_b of solar radiation.

By far the most common instrument that has been used and is likely to be used in the future for measuring I_b is the normal incidence pyrheliometer (NIP). Because it has a field of view characterized by an acceptance half angle 10 times larger than the solar disk itself, it includes a sizable portion of circumsolar radiation. Determination of the distribution of circumsolar radiation is particularly important for collectors with high concentration because their field of view is considerably smaller than that of the pyrheliometer; hence predictions based on pyrheliometer data may overestimate the performance significantly. (For a discussion of the connection between concentration and acceptance angle, see Winston 1970 or Rabl 1976).

Since 1974 a systematic program to measure the distribution of circumsolar radiation has been carried out by the Lawrence Berkeley Laboratory (LBL) (Grether et al. 1977a–d and 1979). Four circumsolar telescopes have been built that scan across the sun to measure the angular brightness distribution $B(\theta)$ (in W/m^2 steradian) with an angular resolution of 1.5 minutes of arc from the center of the sun to 0.5 degrees, and 4.5 minutes of arc from 0.5 to 3.2 degrees. They have been operated at several locations, including Albuquerque, N. Mex.; Argonne, Ill.; Atlanta, Ga.; China Lake, Calif.; and Fort Hood, Tex. For the calculations in this paper, data for all of these locations with a total of about 5 years have been used.

Some analyses of circumsolar radiation are described by Grether et al. (1977a–d and 1979) and Grether and Hunt (1977); these analyses served as a starting point for our investigation. Grether et al. (1977d) evaluated the radiation intercepted by an idealized optical system with a sharply defined field of view (effective aperture radius or acceptance angle) and no optical errors or aberrations. In other studies, Grether et al. (1977c and 1979) calculated the loss of performance due to circumsolar radiation for two specific central receiver designs. Although their calculations provide a very detailed picture of the effects of circumsolar radiation on the performance of these specific optical systems at particular locations (Albuquerque, China Lake, and Fort Hood), the results are difficult to generalize to other concentrator configurations and operating conditions. The goal of our investigation is to develop a simple model of circumsolar effects that is suitable for most solar

concentrator types and operating conditions and is sufficiently accurate for practical purposes.

Before developing such a model, one must determine what is to be learned from it. Basically, there are two questions concerning the effect of circumsolar radiation on concentrating solar collectors. The first is: given the specific sun shape at a particular moment, what is the corresponding <u>instantaneous</u> performance of a concentrating collector? This question is important for verification of the detailed agreement between test data and optical analysis. It requires as input the solar brightness as measured by a circumsolar telescope during the test. The second question concerns the <u>average</u> decrease in performance due to the loss of circumsolar radiation. This is important for system performance prediction and economic analysis. Above all, one needs to know the long-term average effect. The effect on instantaneous performance under a range of operating conditions may also be of interest. For this purpose, accuracy in an average sense is far more important than precise agreement between model and performance for a particular moment. Relaxation of the requirement for detailed agreement in favor of average agreement is very important because it permits greater flexibility in the development of an analytical tool for modeling the effect of circumsolar radiation. Simplicity of the model is desirable to avoid excessive complexity of system performance calculations and to provide intuitive understanding.

In Section 2.0 of this paper the Lawrence Berkeley Laboratory reports are reviewed in order to prepare the basis for the development of the model. The optical analysis used for the calculations is outlined in Section 3.0.

With the formulas in Section 3.0 the instantaneous performance can be calculated within the accuracy of a given circumsolar measurement. This calculation is reasonably fast, requiring only 56 multiplications and additions per scan, provided the optical properties of the collector have been stated in terms of the angular acceptance function. The model for the long-term average effect of circumsolar radiation is developed in Section 4.0, and a correction factor to account for the optical properties of the pyrheliometer is derived in Section 5.0. Numerical results and validation are presented in Section 6.0. The reader who is not interested in the details of our analysis is advised to proceed directly to Section 7.0, where the key results are summarized as a self-contained users' guide.

SERI ⟨≡⟩

SECTION 2.0

REVIEW OF LBL RESULTS

2.1 MAGNITUDE OF CIRCUMSOLAR RATIO

For an indication of the magnitude of circumsolar radiation I_c, it is helpful to look at a plot of beam irradiance I_b vs. ratio I_c/I_b. The latter is approximately equal to the circumsolar ratio

$$R = \frac{I_c}{I_s + I_c} \qquad (2-1)$$

as defined in Grether et al. (1977b) and in the present paper. (I_b is slightly less than $I_s + I_c$ because of the angular acceptance characteristics of the normal incidence pyrheliometer (NIP); see Section 5.0 below.) Many such plots are presented by Grether et al. (1977b). Figure 2-1 (from Grether 1979) for China Lake in February 1977 is quite typical. In this study the upper envelope of the data points is explained by a simple maximum scattering model based on energy conservation. The upper envelope is very closely approximated by the model (solid line) and appears to be a universal feature of circumsolar radiation. This is an important result because it shows that large values of the circumsolar ratio (in excess of 30%) occur only when the beam irradiance is relatively low, i.e., $I_b \lesssim 500 \ W/m^2$. These large circumsolar ratios can be expected to have relatively little effect on average collector performance because most useful energy is collected when $I_b \gtrsim 500 \ W/m^2$.

Many of the data points in Fig. 2-1 cluster around small circumsolar ratios, and the average circumsolar ratio is much smaller than is implied by the upper boundary. An indication of typical average values of the circumsolar ratio is provided by Fig. 2-2 (Grether 1977d, Fig. 20). The ordinate values show how much the pyrheliometer overestimates the radiation available to idealized focusing collectors. The collectors are idealized because they are assumed to have a sharp cutoff θ_c; i.e., they accept all rays incident with $\theta < \theta_c$ and reject all rays with $\theta > \theta_c$. The solid line corresponds to $\theta_c = 0.28°$, the angular radius of the sun. Therefore, this line gives an estimate of the monthly average circumsolar ratio

$$R_{av} = \frac{\overline{I}_c}{\overline{I}_s + \overline{I}_c} \ .$$
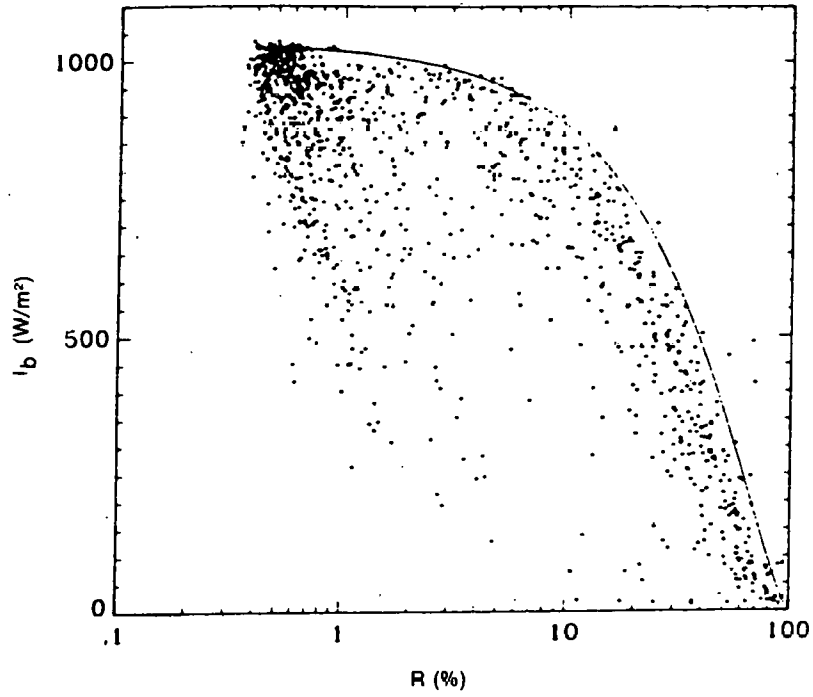
Figure 2-1. Typical Values of Pyrheliometer Reading I_b and Circumsolar Ratio R Shown with Boundary Derived by Grether [1979].
China Lake, Calif; February 1977; all sky conditions

SERI
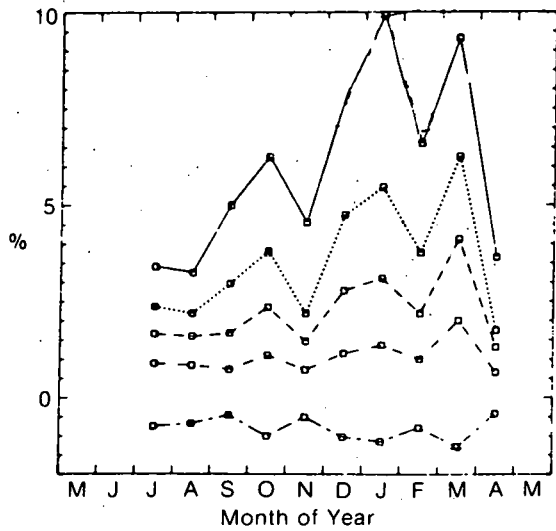
(a) Threshold = 0 W/m²

EFF Aperture Radius

———— 0.28° (4.8 mrad)
············· 0.38° (6.5 mrad)
— — — 0.80° (14.0 mrad)
— · — · 1.63° (28.4 mrad)
— · · — 3.20° (55.9 mrad)
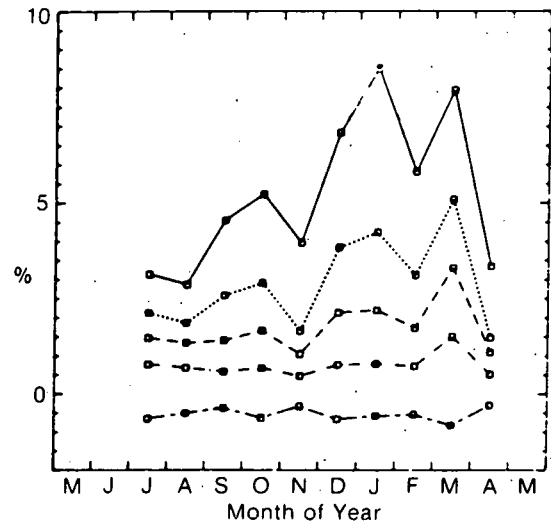
(b) Threshold = 50 W/m²

(c) Threshold = 150 W/m²
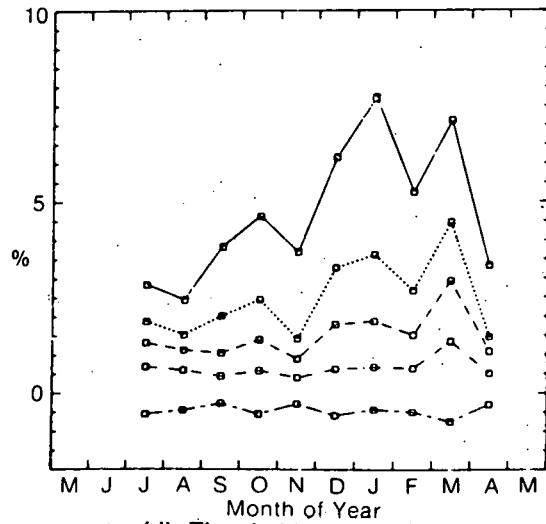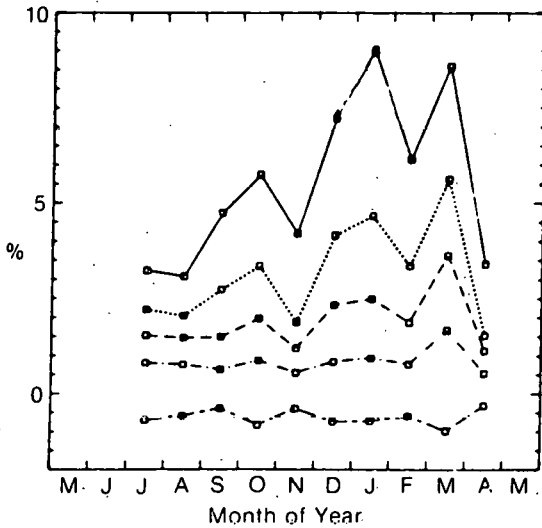
(d) Threshold = 300 W/m²
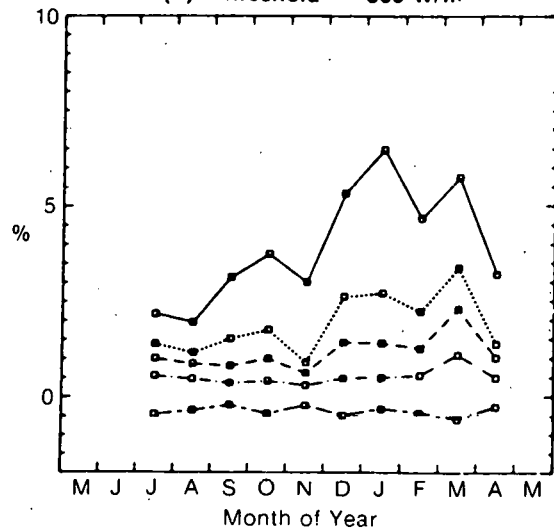
(e) Threshold = 500 W/m²

Figure 2-2. Overestimate of Pyrheliometer (NIP) in % at Fort Hood, Tex., 1976-77, for All Sky Conditions. From Grether et al. 1977d

(The θ_c = 3.20° curve corresponds to negative overestimate because the pyrheliometer has a field of view smaller than 3.20°.)

Five graphs are presented for five values of the operating threshold: q = 0, 50, 150, 300, and 500 W/m². Figure 2-2a, for zero threshold, shows that the monthly average circumsolar ratio at Fort Hood ranges from a low of 3.5% in summer to a high of 10% in winter. Systems with nonzero threshold are turned on only when the insolation is above the threshold; therefore, periods of low insolation, which tend to be associated with higher circumsolar ratios, are excluded from the computation of R_{av}. This explains why the effective circumsolar ratio in Figs. 2-2b through 2-2e decreases with threshold.

The magnitude and seasonal variation of average circumsolar ratio depends on location. Of particular interest is the fact that even at a location like Fort Hood, which has relatively high circumsolar levels, the monthly average circumsolar ratio does not exceed 10%. It seems that occurrences of high circumsolar radiation are sufficiently rare to keep the average circumsolar ratio well below the boundary in Fig. 2-1.

The variation of the effective circumsolar ratio $R_{av}(q)$ with threshold q is exhibited more clearly by Fig. 2-3, where some of the data of Fig. 2-2 have been replotted versus q. The crosses, connected by solid lines, represent the points of Fig. 2-2 for θ_c = 0.28° for several months. The crosses are well correlated by a straight line that passes through a circumsolar ratio of approximately 1% to 3% at a threshold of 1000 W/m². This limiting value of approximately 1% to 3% depends on location and time of year and corresponds to typical circumsolar ratios on very clear days. Figure 2-3 suggests a simple linear relationship for the variation of the effective average circumsolar ratio $R_{av}(q)$ with threshold q. This general pattern persists when collectors with different acceptance angles are considered. For example, the circles connected by dotted lines in Fig. 2-3 show that the θ_c = 0.8° points of Fig. 2-2 also decrease linearly with threshold q.

2.2 INTERCEPTED RADIATION

Another feature of Fig. 2-2 is that the "overestimate of NIP" for all systems with an acceptance half angle θ_c between 0.28° and 2.8° tends to be proportional to R_{av}. This general behavior is found also in the analysis of realistic collectors; e.g., the central receiver (Grether et al. 1977c). To simplify the circumsolar analysis of the central receiver, Grether and Hunt (1977) selected 16 standard circumsolar scans such that the shape of any real scans could be approximated by one of these 16. Normalized to unity at θ = 0, the brightness distribution B(θ) for these standard scans is plotted in Fig. 2-4 versus angle θ from the center of the sun.

Figure 2-5 shows for the 16 standard scans the fraction F of the irradiance $I_s + I_c$ that is lost by the central receiver designs proposed by Martin Marietta and McDonnell Douglas. F is defined such that

SERI
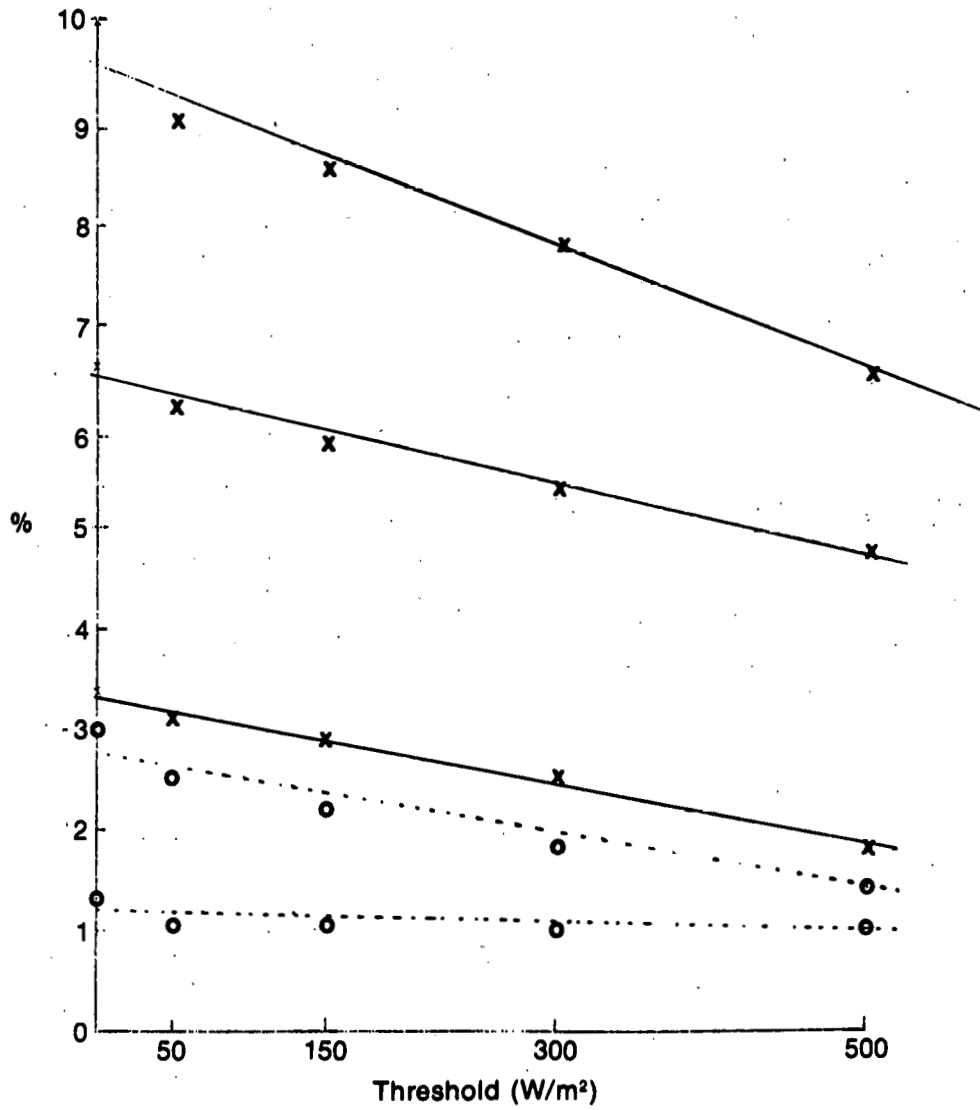
Figure 2-3. Some Selected Points from Figure 2-2 Replotted to Show Variation of Overestimate of Pyrheliometer with Threshold.
Fields of view of 0.28° (solid lines) and 0.80° (dashed lines)
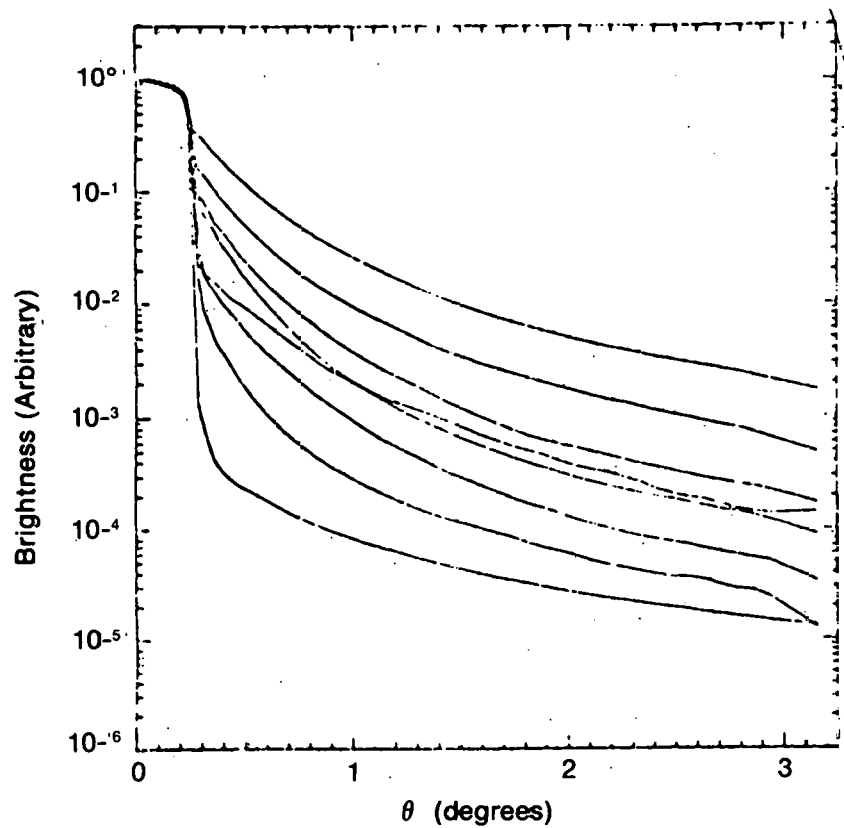
(a) Telescope 2 (Albuquerque)
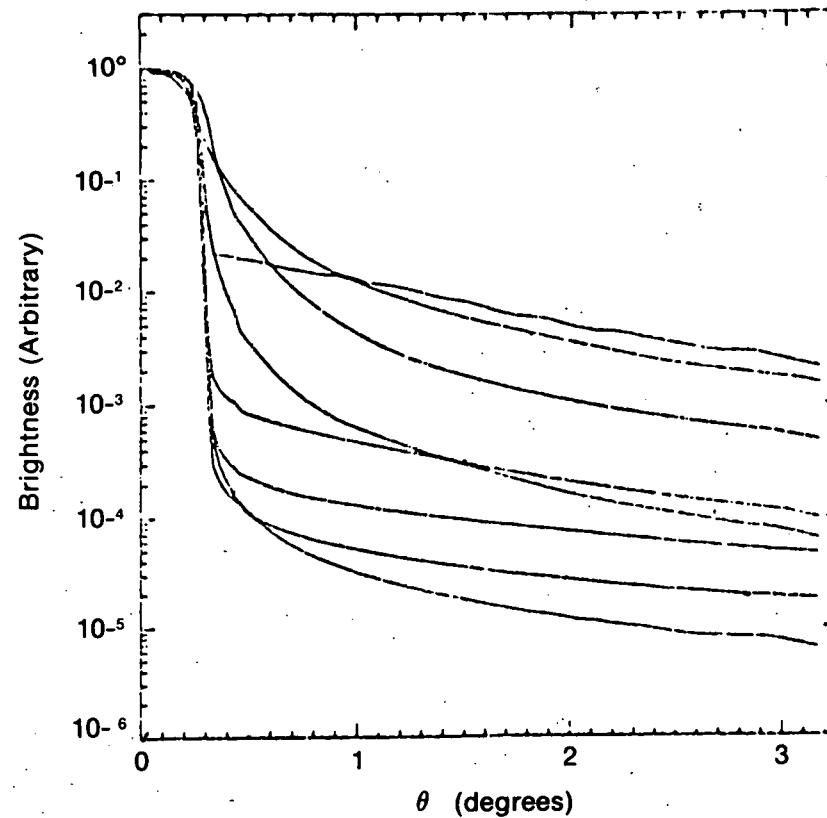
(b) Telescope 3 (Ft. Hood)

Figure 2-4. Sixteen Standard Circumsolar Scans of LBL
From Grether and Hunt 1977. Standard profiles (normalized)

SERI
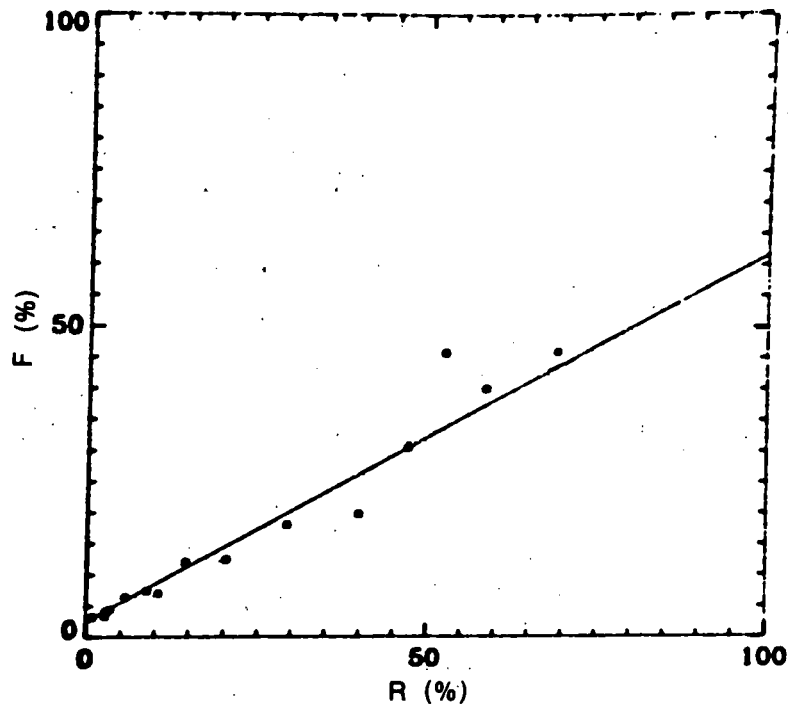
(a) Martin Marietta Pilot Design
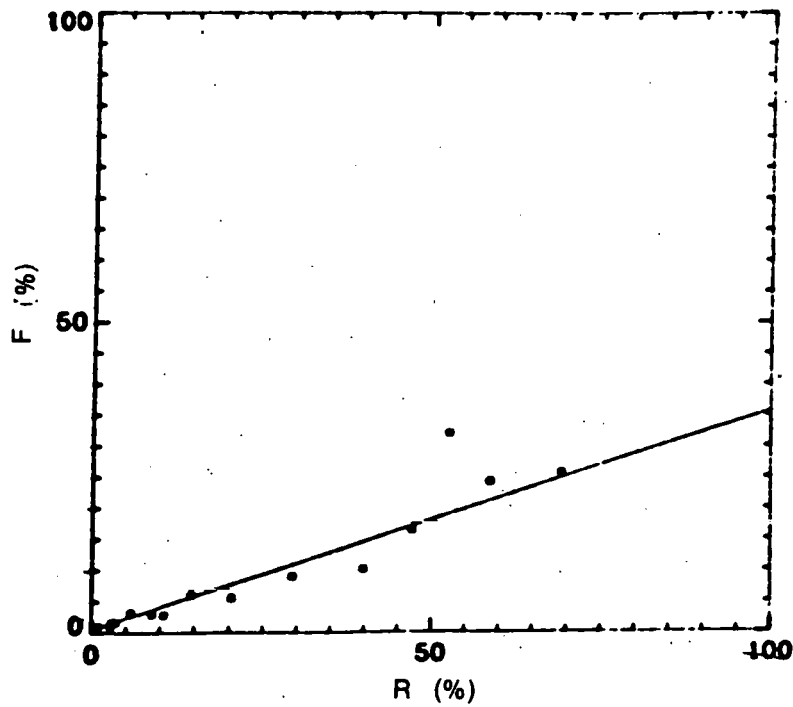
(b) McDonnell Douglas Pilot Design

Figure 2-5. Fraction F of Available Beam Insolation Lost Versus Circumsolar
Ratio R for 16 Standard LBL Scans for Two Central Receiver Designs

$$I_{in} = (1 - F) (I_s + I_c) \qquad (2-2)$$

is the amount of radiation intercepted by the receiver when the solar plus circumsolar radiation is $I_s + I_c$. F includes all optical errors and aberrations but no absorption losses; hence, F depends only on concentrator geometry and sun shape. Figure 2-5 suggests an approximately linear correlation between F and the circumsolar ratio:

$$F = \bar{F}_o + F' \frac{I_c}{(I_s + I_c)} , \qquad (2-3)$$

where F_o and F' depend on the optics of the collector but are independent of insolation. Combining Eqs. 2-2 and 2-3 yields

$$I_{in} = (1 - F_o) (I_s + I_c) - F' I_c ; \qquad (2-4)$$

thus a constant fraction F' of circumsolar radiation is lost. This phenomenon is verified by the results of the detailed simulations that are shown in Fig. 2-6 (Grether et al. 1977c, Fig. 7) as the fraction of circumsolar radiation I_c that is lost. For the two central receiver designs and for idealized optics with various acceptance half angles, the fraction of I_c that is lost depends only weakly (at most ± 10% relative variation) on season and location.

The near constancy of the curves in Fig. 2-6 suggests that Eq. 2-3 may actually be a very good correlation when averaged over a large number of solar scans, even though the points for the 16 standard LBL scans in Fig. 2-5 deviate considerably from the straight line. The large deviations are not surprising because the 16 standard scans were not selected to be representative of any possible correlations between sun shape, circumsolar ratio, and beam insolation. The deviation from the straight line is particularly strong for high circumsolar ratios, but this is of little concern since high circumsolar ratios are not associated with significant amounts of collectible energy.

For the remainder of this paper it is more convenient to work with the intercept factor

$$\gamma_{sc} = \frac{I_{in}}{I_s + I_c} ; \qquad (2-5)$$

($\gamma_{sc} = 1 - F$ in the notation of Grether et al. 1977c). Equation 2-4 is a model for the instantaneous performance corresponding to a particular circumsolar scan; however, as a linear equation in $I_s + I_c$ and I_{in}, it also holds

SERI ⬡
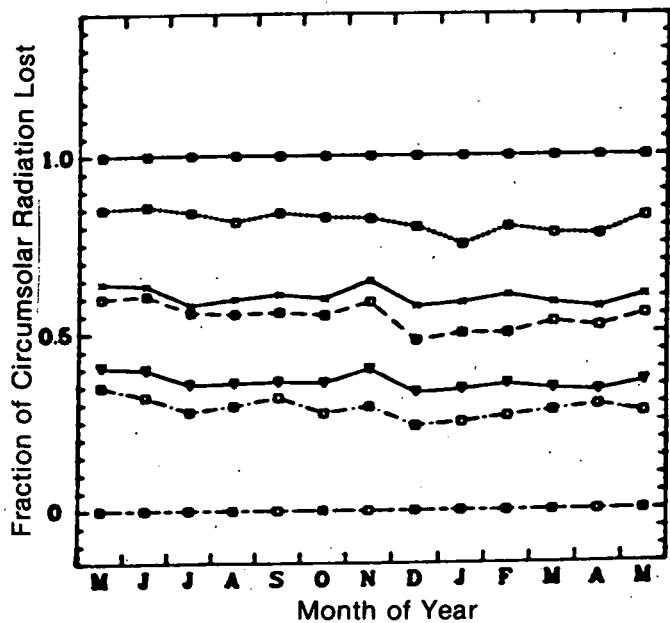
(a) Albuquerque, N. Mex.
1976-77
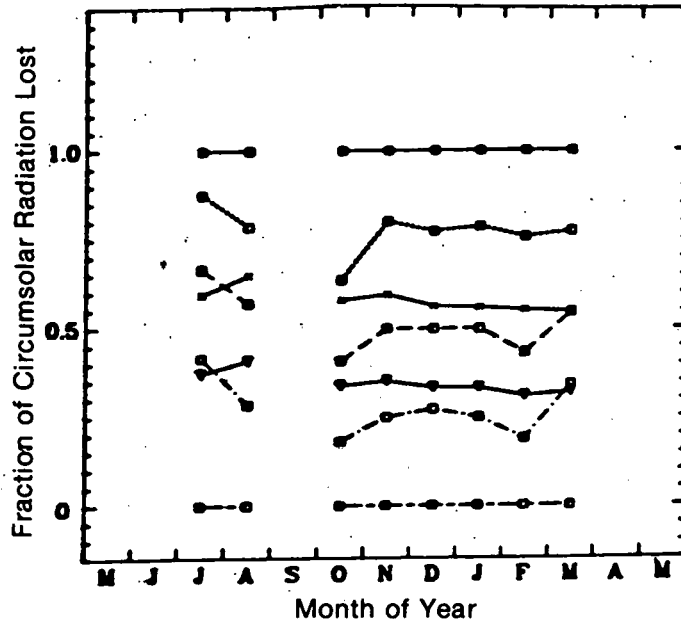
(b) China Lake, Calif.
1976-77
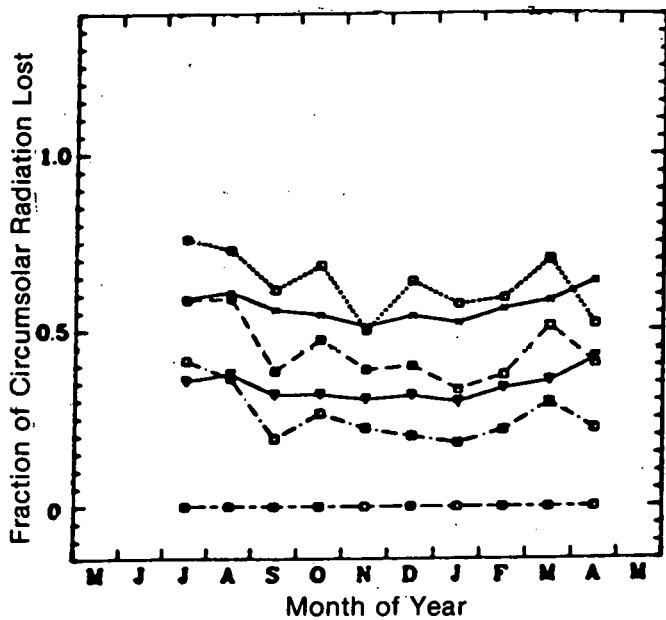
EFF Aperture Radius

□———□	0.28° (4.8 mrad)
□········□	0.38° (6.5 mrad)
□—— —□	0.80° (14.0 mrad)
□—·—·—□	1.63° (28.4 mrad)
□——·—□	3.20° (55.9 mrad)

✕——✕	Martin Marietta Pilot
△——△	McDonnell Douglas Pilot

(c) Ft. Hood, Tex.
1976-77

Figure 2-6. Fraction of Average Circumsolar Radiation Lost by Two Central Receiver Designs and by Five Collectors with Different Effective Apertures. Threshold = 50 W/m²

true when the insolation values are time averaged irrespective of the frequency distributions. Figure 2-6 and Eq. 2-4 suggest the following simple model for calculating the average effect of circumsolar radiation. The long-term average intercept factor

$$\gamma_{sc,av} = \frac{\overline{I}_{in}}{\overline{I}_s + \overline{I}_c} \qquad (2-6)$$

is given by an expression of the form

$$\gamma_{sc,av} = (1 - F_o) - F' R_{av}(q) , \qquad (2-7)$$

where $R_{av}(q)$ is the effective average circumsolar ratio corresponding to a threshold q and given in Fig. 2-3. The coefficients $(1 - F_o)$ and F' depend on the optics of the collector but not on insolation. $(1 - F_o)$ is the intercept factor for a perfectly clear sky $(I_c = 0)$. The questions that remain to be investigated in this paper are: how accurate is this model, and how does one calculate $(1 - F_o)$ and F'?

SECTION 3.0

OPTICAL ANALYSIS

The crucial quantity to be calculated in this paper is the intercept factor γ_{sc} of Eq. 2-5. Once γ_{sc} is known, the radiation q_{abs} absorbed by the receiver is obtained by multiplying the intercepted radiation $I_{in} = \gamma_{sc}(I_s + I_c)$ by the effective reflectance-transmittance-absorptance product $(\rho\tau\alpha)$ of the collector:

$$q_{abs} = (\rho\tau\alpha)\, \gamma_{sc}\, (I_s + I_c) \ . \tag{3-1}$$

For thermal collectors, the efficiency is found by subtracting heat loss q_{loss} (in W/m^2 per aperture area) and normalizing by $I_s + I_c$:

$$\eta = (q_{abs} - q_{loss})/(I_s + I_c)$$
$$= (\rho\tau\alpha)\, \gamma_{sc} - q_{loss}/(I_s + I_c) \tag{3-2}$$

For the calculation* of γ_{sc} it is convenient to define the angular acceptance function $f(\theta)$ as that fraction of a uniform beam of parallel rays incident on the aperture at an angle θ from the optical axis that reaches the receiver if the optics are perfect. This function accounts for aberrations of a perfect parabola at the nonzero incidence angle θ but does not include optical errors. For a parabolic dish with a flat receiver, the calculation of $f(\theta)$ is quite tedious (Bendt and Rabl 1979), but the results can be approximated with sufficient accuracy by a second-order polynomial in $C\theta^2$:

$$f(\theta) = \begin{cases} 1 & \text{for } \sqrt{C}\theta < v_1 \\ a + bC\theta^2 + c(C\theta^2)^2 & \text{for } v_1 < \sqrt{C}\theta < v_2 \\ 0 & \text{for } \sqrt{C}\theta > v_2 \end{cases} \ . \tag{3-3}$$

C is the geometric concentration ratio, and the coefficients a, b, c, v_1, and v_2 depend only on the rim angle ϕ; they are tabulated in Bendt and Rabl (1979).

Seen through the optics of the collector, the sun appears smeared because of optical errors. These arise from deviations of the reflector contour from the

---

*In the interest of brevity, some details are omitted that are explained in Bendt and Rabl 1979 and Bendt et al. 1979.

design shape, lack of perfect specularity of the reflector surface, displacement of the receiver relative to the reflector, and incorrect tracking. Even though the individual error distributions may not be exactly Gaussian, their combination can be approximated, in most cases, by a Gaussian distribution of width σ, the rms angular standard deviation of a reflected ray from its design direction.

The intercept factor is the convolution of the angular acceptance function $f(\theta)$, the optical error distribution, and the angular brightness distribution $B(\theta)$ of the sun. To carry out the calculations in this paper it is most convenient to define a function $f_\sigma(\theta)$ as the convolution of $f(\theta)$ with the error distribution:

$$f_\sigma(\theta) = \frac{1}{2\pi\sigma^2} \iint_{-\infty}^{\infty} f\left[\left(\theta_x^2 + \theta_y^2\right)^{1/2}\right] \exp\left(-\frac{(\theta - \theta_x)^2 + \theta_y^2}{2\sigma^2}\right) d\theta_x\, d\theta_y \quad . \quad (3\text{-}4)$$

The function $f_\sigma(\theta)$, the "smeared angular acceptance function," is the fraction of a parallel and uniform beam of radiation incident on the aperture of a real collector with optical errors that reaches the receiver. The intercept factor is simply the product of $f_\sigma(\theta)$ and the normalized brightness distribution $B(\theta)/(I_s + I_c)$, integrated over all angles θ:

$$\gamma_{sc} = \frac{2\pi}{(I_s + I_c)} \int_0^\Delta \theta\, f_\sigma(\theta)\, B(\theta)\, d\theta \quad . \quad (3\text{-}5)$$

The intercept factor γ_{sc} can be computed quickly for a large number of circumsolar scans if $f_\sigma(\theta)$ is calculated once for each set of concentrator parameters and for each of the angles at which $B(\theta)$ is measured and if it is then stored in the computer memory.

The angular acceptance function for the line focus case is given in Bendt et al. (1979). The expression analogous to Eq. 3-4 is

$$f_{\sigma,\text{line}}(\theta) = \frac{1}{\sqrt{2\pi}\sigma} \int_{-\infty}^{\infty} f(\theta - \theta') \exp\left(-\frac{\theta'^2}{2\sigma^2}\right) d\theta' \quad . \quad (3\text{-}6)$$

The intercept factor can be computed by transforming the circumsolar scan to linear geometry

$$\gamma_{sc,line} = \frac{4}{(I_s + I_c)} \int_0^\Delta f_{\sigma,line}(\theta_x) \, d\theta_x \int_0^\Delta B\left[\left(\theta_x^2 + \theta_y^2\right)^{1/2}\right] d\theta_y \quad . \tag{3-7}$$

If the calculation is to be repeated for many scans, however, it is faster to transform the smeared angular acceptance function $f_{\sigma,line}(\theta)$ to point focus geometry by averaging it over azimuthal directions. The result

$$f_{\sigma,equiv}(\theta) = \frac{1}{2\pi} \int_0^{2\pi} f_{\sigma,line}(\theta \cos \phi) \, d\phi \tag{3-8}$$

is the equivalent smeared point focus acceptance function of a line focus collector and, therefore, can be used directly in Eq. 3-5.

If an accurate system simulation is needed and if circumsolar data of the LBL type are available, we recommend that Eq. 3-5 be used to calculate the instantaneous collector efficiency corresponding to each scan. Since the LBL data are given as brightness values at 56 angular intervals, such a calculation requires only 56 multiplications and additions for each scan, assuming, of course, that $\theta f_\sigma(\theta)$ has been previously calculated and stored in memory.* The angular acceptance function and hence $f_\sigma(\theta)$ can be readily calculated for any concentrator using either ray tracing or the analytical technique described in Bendt and Rabl (1979), which is much faster and more accurate.

---

*For the central receiver f_σ may vary slightly with the zenith and azimuth of the sun, in which case several functions have to be stored.

SERI☼

SERI 🏵

SECTION 4.0

THE PHYSICS OF THE LINEAR MODEL

To understand the linear form of Eq. 2-4 and to motivate our own analysis, it is instructive to take another look at the 16 standard scans in Fig. 2-4. These scans can be characterized as a nearly uniform solar disk with a sharp edge around 4.7 mrad, followed by a circumsolar tail which has a similar shape for all scans. The brightness in the circumsolar region varies from scan to scan, but the relative change of brightness with angle is not very different; in other words, the curves run fairly parallel in the circumsolar region. Mathematically, such behavior can be described by a brightness function of the form

$$
B(\theta) = \begin{cases} \beta_s(\theta) & \text{for} \quad \theta < \delta \approx 4.7 \text{ mrad} \\[2ex] a\beta_c(\theta) & \text{for} \quad \theta > \delta \approx 4.7 \text{ mrad} \quad, \end{cases} \tag{4-1}
$$

where the constant a is related to the circumsolar ratio R.

The corresponding solar disk irradiance is

$$
I_s = 2\pi \int_0^\delta \theta \beta_s(\theta) \, d\theta \quad, \tag{4-2}
$$

and the circumsolar irradiance is

$$
I_c = 2\pi \, a \int_\delta^\Delta \theta \beta_c(\theta) \, d\theta \quad. \tag{4-3}
$$

In terms of the circumsolar ratio $R = I_c/(I_s + I_c)$, the constant a is given by

$$
a = \frac{R \int_0^\delta \theta \beta_s(\theta) \, d\theta}{(1 - R) \int_\delta^\Delta \theta \beta_c(\theta) \, d\theta} \quad. \tag{4-4}
$$

17

S≡RI

Now Eq. 3-5 is used to calculate the intercept factor

$$\gamma_{sc} = \frac{I_{in}}{I_s + I_c}$$

corresponding to this brightness distribution:

$$\gamma_{sc} = \frac{2\pi}{(I_s + I_c)} \left(\int_0^{\delta} \theta\beta_s(\theta) \, f_\sigma(\theta) \, d\theta + a\int_{\delta}^{\Delta} \theta\beta_c(\theta) \, f_\sigma(\theta) \, d\theta \right) \quad . \quad (4\text{-}5)$$

It is convenient to define a quantity

$$\gamma_s = \frac{2\pi}{I_s} \int_0^{\delta} \theta\beta_s(\theta) \, f_\sigma(\theta) \, d\theta \qquad (4\text{-}6)$$

as the intercept factor for radiation from the solar disk, and an analogous quantity, which is independent of a,

$$\gamma_c = \frac{2\pi a}{I_c} \int_{\delta}^{\Delta} \theta\beta_c(\theta) \, f_\sigma(\theta) \, d\theta \qquad (4\text{-}7)$$

as the intercept factor for circumsolar radiation. In terms of γ_s and γ_c, Eq. 4-5 can be written as

$$\gamma_{sc} = \frac{\gamma_s I_s + \gamma_c I_c}{I_s + I_c} \quad , \qquad (4\text{-}8)$$

which has a simple physical interpretation. The intercept factor γ_{sc} is the weighted average of the intercept factor γ_s for the solar disk and the intercept factor γ_c for the circumsolar region. By inserting the circumsolar ratio R, one can rearrange Eq. 4-8 in a slightly more convenient form:

$$\gamma_{sc} = \gamma_s - \left(\gamma_s - \gamma_c\right) R \quad , \qquad (4\text{-}9)$$

which is precisely the linear model (Eq. 2-4) suggested by the analysis of Grether et al. For the instantaneous performance associated with a particular circumsolar scan, this equation is a rather crude model, as shown by the scatter of data points about the trend line in Fig. 2-5 and as expected from the fact that individual circumsolar scans can deviate significantly from the average shape suggested by Fig. 2-4. This is of little concern, however, since the instantaneous performance for a particular scan can be calculated readily from Eqs. 3-5 or 3-7.

The linear model does turn out to be remarkably accurate for predicting the long-term average performance; therefore, we proceed to derive the equivalent of Eq. 4-9 for the calculation of the long-term average. The long-term average irradiance $\overline{I}$ is defined as the average over a large number N of data

$$\overline{I} = \frac{1}{N} \sum_{i=1}^{N} {}_+ I(i) \tag{4-10}$$

with appropriate subscripts indicating solar, circumsolar, and intercepted components. The subscript plus sign under the summation sign means that only those periods with intercepted irradiance above a specified threshold q are to be included. The average could be defined for any time period (e.g., a year, a month, a time of day) and, ideally, it should be calculated from many years' worth of data. Because a model for predicting the long-term average intercepted irradiance $\overline{I}_{in}$ is desired, given the long-term average solar and circumsolar irradiance $\overline{I}_s + \overline{I}_c$, an average intercept factor is defined as

$$\gamma_{sc,av} \equiv \frac{\overline{I}_{in}}{\overline{I}_s + \overline{I}_c} . \tag{4-11}$$

In contrast to the bar notation for genuine averages, the subscript "av" designates ratios of averages in this paper. Retracing the steps from Eq. 4-5 to Eq. 4-9 yields an expression for $\gamma_{sc,av}$ of the same form as Eq. 4-9:

$$\gamma_{sc,av} = \gamma_{s,av} - (\gamma_{s,av} - \gamma_{c,av}) R_{av} , \tag{4-12}$$

where R_{av} is the long-term average circumsolar ratio

$$R_{av} \equiv \frac{\overline{I}_c}{\overline{I}_s + \overline{I}_c} \tag{4-13}$$

and $\gamma_{s,av}$ and $\gamma_{c,av}$ are defined as

$$\gamma_{s,av} \equiv \frac{2\pi}{\overline{I}_s} \int_0^{\delta} \theta \, \overline{B}(\theta) \, f_\sigma(\theta) \, d\theta \tag{4-14}$$

and

$$\gamma_{c,av} \equiv \frac{2\pi}{\bar{I}_c} \int_\delta^\Delta \theta \, \bar{B}(\theta) \, f_\sigma(\theta) \, d\theta \quad . \tag{4-15}$$

The long-term average irradiance from the solar disk,

$$\bar{I}_s = 2\pi \int_0^\delta \theta \, \bar{B}(\theta) \, d\theta \quad , \tag{4-16}$$

is the integral over the disk of the long-term average brightness distribution

$$\bar{B}(\theta) = \frac{1}{N} \sum_{i=1}^{N} {}_+ B_i(\theta) \quad , \tag{4-17}$$

and analogously the average circumsolar irradiance is

$$\bar{I}_c = 2\pi \int_\delta^\Delta d\theta \, \theta \, \bar{B}(\theta) \quad . \tag{4-18}$$

Equation 4-12 is a tautology when used with only a single set of data. The equation is useful because an excellent approximation can be obtained for any set of circumsolar data at any location or time or threshold if $\gamma_{s,av}$ and $\gamma_{c,av}$ are calculated for a <u>single synthetic circumsolar scan</u>. For this synthetic scan, we take the average over all the circumsolar scans supplied by Lawrence Berkeley Laboratory. This average scan $\bar{B}(\theta)$ is tabulated in Table 4-1 for point focus geometry and in Table 4-2 for line focus geometry; it is plotted in Fig. 4-1.*

The fact that the brightness of the disk decreases somewhat with θ is called "limb darkening." Analytical expressions for the limb-darkening effect have been published in many places; e.g., Biggs and Vittitoe (1979). However, they were based on only a few measurements and therefore are not necessarily reliable as descriptions of the average brightness distribution. The simulations reported in Section 6.0 show that the average distribution $\bar{B}(\theta)$ in

---

*A peculiarity of the circumsolar data corresponding to high circumsolar ratios is a very slight increase in brightness at the edge of the scan. Assuming that this unphysical behavior is due to inaccuracies at the edge of the operating range of the circumsolar telescope, we have corrected the last two entries (53.887 mrad and 55.196 mrad) by extrapolation from smaller angles.

SERI ⬡

Table 4-1. STANDARD SOLAR SCAN FOR POINT FOCUS GEOMETRY[a]

θ (mrad)	$\overline{B}(\theta)$ (W/m^2 sterad)[b]		w_s	w_c[c]
0.218	13,631,252		8.7618E-10	0
0.654	13,561,148		2.6285E-09	0
1.091	13,441,701		4.3809E-09	0
1.527	13,263,133		6.1333E-09	0
1.963	13,012,331		7.8856E-09	0
2.400	12,668,456	Solar	9.6380E-09	0
2.836	12,185,726	Disk	1.1390E-08	0
3.272	11,443,798		1.3148E-08	0
3.709	10,061,047		1.4895E-08	0
4.145	7,002,494		1.6647E-08	0
4.581	1,730,196		1.8400E-08	0
5.018	144,818		0	5.3801E-07
5.454	63,325		0	5.8489E-07
5.890	51,116		0	6.3158E-07
6.327	43,669		0	6.7837E-07
6.763	36,973		0	7.2515E-07
7.199	31,935		0	7.7193E-07
7.636	27,979		0	8.1872E-07
8.072	24,767		0	8.6550E-07
8.508	21,830		0	9.1229E-07
9.381	17,444		0	3.0176E-06
10.690	13,084		0	3.4386E-06
11.999	10,194		0	3.8597E-06
13.308	8,177		0	4.2807E-06
14.617	6,716		0	4.7018E-06
15.926	5,634		0	5.1228E-06
17.235	4,807		0	5.5439E-06
18.544	4,147	Circumsolar	0	5.9649E-06
19.853	3,633	Region	0	6.3860E-06
21.162	3,213		0	6.8071E-06
22.471	2,867		0	7.2281E-06
23.780	2,579		0	7.6492E-06
25.089	2,337		0	0.0702E-06
26.398	2,133		0	8.4913E-06
27.707	1,958		0	8.9123E-06
29.016	1,805		0	9.3334E-06
30.325	1,672		0	9.7544E-06
31.634	1,550		0	1.0175E-05
32.943	1,444		0	1.0597E-05
34.252	1,353		0	1.1018E-05
35.561	1,268		0	1.1439E-05
36.870	1,194		0	1.1860E-05
38.179	1,127		0	1.2281E-05
39.488	1,070		0	1.2702E-05
40.797	1,018		0	1.3123E-05
42.106	969		0	1.3544E-05

Break in size of angular interval → (at 8.508)

Table 4-1. STANDARD SOLAR SCAN FOR POINT FOCUS GEOMETRY[a]
(concluded)

θ (mrad)	$\overline{B}(\theta)$ (W/m^2 sterad)[b]		w_s	w_c [c]
43.415	923		0	1.3965E-05
44.724	882		0	1.4386E-05
46.033	845		0	1.4807E-05
47.342	811		0	1.5228E-05
48.651	777	Circumsolar	0	1.5648E-05
49.960	747	Region	0	1.6070E-05
51.269	722		0	1.6491E-05
52.578	700		0	1.6912E-05
53.887	681		0	1.7333E-05
55.196	665		0	1.7754E-05

[a]Solar radius 0.275° (disk plus resolution of instrument).

[b]Brightness at angle θ from center of sun.

[c]Weighting factors w_s of Eq. 7-6 and w_c of Eq. 7-7 (in sterad m^2/W).

SERI

Table 4-2. STANDARD SOLAR SCAN FOR LINE FOCUS GEOMETRY

θ (min)	θ (mrad)	Solar Disk (W/m² rad)	Circumsolar Region (W/m² rad)
0.75	0.218	106,068	683
2.25	0.654	104,517	686
3.75	1.091	101,495	691
5.25	1.527	96,954	698
6.75	1.963	90,534	710
8.25	2.400	82,146	724
9.75	2.836	71,666	743
11.25	3.272	58,326	776
12.75	3.709	41,574	824
14.25	4.145	22,944	907
15.75	4.581	7,978	1,039
17.25	5.018	0	1,085
18.75	5.454	0	954
20.25	5.890	0	816
21.75	6.327	0	742
23.25	6.763	0	681
24.75	7.199	0	628
26.25	7.636	0	584
27.75	8.072	0	545
29.25	8.508	0	511
30.75	8.945	0	481
32.25	9.381	0	454
33.75	9.817	0	429
35.25	10.254	0	407
36.75	10.690	0	387
38.25	11.126	0	369
39.75	11.563	0	352
41.25	11.999	0	337
42.75	12.435	0	323
44.25	12.872	0	310
45.75	13.308	0	298
47.25	13.744	0	287
48.75	14.181	0	276
50.25	14.617	0	267
51.75	15.053	0	258
53.25	15.490	0	249
54.75	15.926	0	241
56.25	16.362	0	234
57.75	16.799	0	227
59.25	17.235	0	220

SERI

Table 4-2. STANDARD SOLAR SCAN FOR LINE FOCUS GEOMETRY
(continued)

θ (min)	θ (mrad)	Solar Disk (W/m² rad)	Circumsolar Region (W/m² rad)
60.75	17.671	0	214
62.25	18.108	0	207
63.75	18.544	0	202
65.25	18.980	0	196
66.75	19.417	0	191
68.25	19.853	0	186
69.75	20.289	0	181
71.25	20.726	0	176
72.75	21.162	0	172
74.25	21.598	0	168
75.75	22.035	0	164
77.25	22.471	0	160
78.75	22.907	0	156
80.25	23.344	0	153
81.75	23.780	0	149
83.25	24.216	0	146
84.75	24.653	0	143
86.25	25.089	0	139
87.75	25.525	0	136
89.25	25.962	0	133
90.75	26.398	0	131
92.25	26.834	0	128
93.75	27.271	0	125
95.25	27.707	0	123
96.75	28.143	0	120
98.25	28.580	0	118
99.75	29.016	0	115
101.25	29.452	0	113
102.75	29.889	0	111
104.25	20.325	0	108
105.75	30.761	0	106
107.25	31.198	0	104
108.75	31.634	0	102
110.25	32.070	0	100
111.75	32.507	0	98
113.25	32.943	0	96
114.75	33.379	0	94
116.25	33.816	0	92
117.75	34.252	0	91
119.25	34.688	0	89

Table 4-2. STANDARD SOLAR SCAN FOR LINE FOCUS GEOMETRY
(continued)

θ (min)	(mrad)	Solar Disk $(W/m^2 \ rad)$	Circumsolar Region $(W/m^2 \ rad)$
120.75	35.125	0	87
122.25	35.561	0	85
123.75	35.997	0	83
125.25	36.434	0	82
126.75	36.870	0	80
128.25	37.306	0	78
129.75	37.743	0	77
131.25	38.179	0	75
132.75	38.615	0	74
134.25	39.052	0	72
135.75	39.488	0	71
137.25	39.924	0	69
138.75	40.361	0	68
140.25	40.797	0	66
141.75	41.233	0	65
143.25	41.670	0	64
144.75	42.106	0	62
146.25	42.542	0	60
147.75	42.979	0	59
149.25	43.415	0	58
150.75	43.851	0	56
152.25	44.288	0	54
153.75	44.724	0	53
155.25	45.160	0	52
156.75	45.597	0	50
158.25	46.033	0	49
159.75	46.469	0	48
161.25	46.906	0	46
162.75	47.342	0	45
164.25	47.778	0	44
165.75	48.215	0	42
167.25	48.651	0	40
168.75	49.087	0	39
170.25	49.524	0	37
171.75	49.960	0	36
173.25	50.396	0	35
174.75	50.833	0	33
176.25	51.269	0	32
177.75	51.705	0	30
179.25	52.142	0	29

SERI

Table 4-2. STANDARD SOLAR SCAN FOR LINE FOCUS GEOMETRY
(concluded)

θ		Solar Disk	Circumsolar Region
(min)	(mrad)	$(W/m^2 \; rad)$	$(W/m^2 \; rad)$
180.75	52.578	0	27
182.25	53.014	0	26
183.75	53.451	0	24
185.25	53.877	0	23
186.75	54.323	0	21
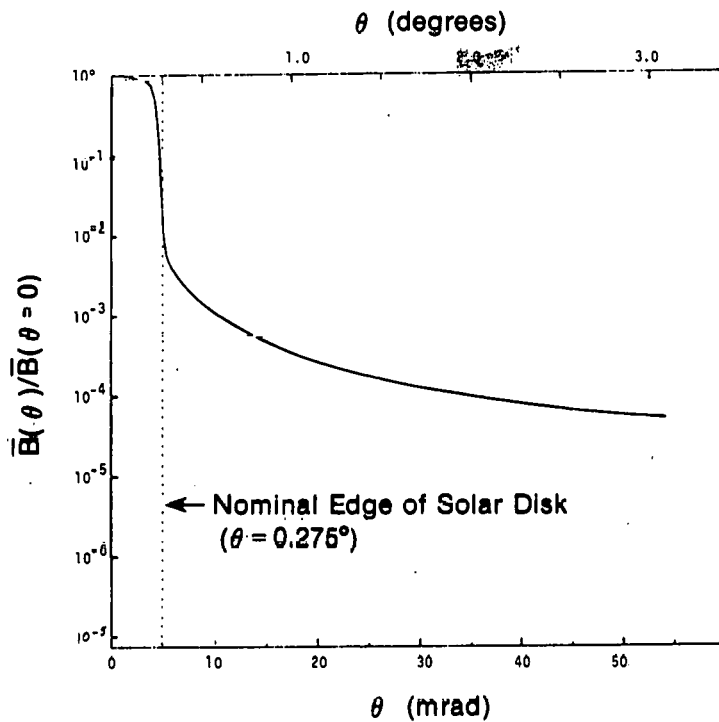
Figure 4-1. Brightness Distribution (in Relative Units) of Standard Circumsolar Scan

Table 4-1 will predict the intercept factor γ_s for the solar disk with an rms error of about 0.0002. The solar disk portion of the distribution in Table 4-1, therefore, is recommended as the best available brightness distribution for the limb- darkened solar disk.

The validity of the linear model in Fig. 2-3 for the threshold dependence of the average circumsolar ratio $R_{av}(q)$ is shown by Table 4-3, where $R_{av}(q)$ for each of the files in the LBL data set is listed for various thresholds q.

Table 4-3. MONTHLY AVERAGE CIRCUMSOLAR RATIO $R_{av}(q)$ VERSUS THRESHOLD q FOR EACH FILE

File	Location	Yr/Mo	Hours of Data	q (W/m²) 0	50	150	300	500
1	Atlanta	77/06	163	0.081	0.078	0.070	0.057	0.039
		77/07	251	0.063	0.059	0.051	0.041	0.026
		77/08	273	0.109	0.100	0.083	0.060	0.039
		77/09	123	0.076	0.071	0.058	0.043	0.024
		77/10	246	0.036	0.034	0.031	0.027	0.019
		77/11	103	0.039	0.033	0.029	0.020	0.013
		77/12	73	0.049	0.044	0.034	0.022	0.018
2	Atlanta	78/01	191	0.057	0.051	0.045	0.034	0.022
		78/02	234	0.055	0.049	0.044	0.033	0.023
		78/03	228	0.043	0.040	0.037	0.030	0.025
		78/04	135	0.068	0.064	0.056	0.050	0.039
		78/05	173	0.050	0.045	0.033	0.023	0.018
		78/06	216	0.071	0.066	0.061	0.050	0.031
3	Albq.	76/05	80	0.021	0.020	0.019	0.016	0.015
		76/06	318	0.029	0.028	0.025	0.022	0.018
		76/07	199	0.027	0.026	0.024	0.017	0.014
		76/08	326	0.032	0.031	0.028	0.025	0.020
		76/09	106	0.040	0.039	0.037	0.027	0.019
		76/10	297	0.040	0.039	0.035	0.030	0.021
		76/11	260	0.024	0.024	0.023	0.022	0.017
		76/12	254	0.036	0.035	0.033	0.029	0.024
4	Albq.	77/01	254	0.040	0.037	0.031	0.023	0.017
		77/02	242	0.046	0.045	0.040	0.036	0.028
		77/03	59	0.060	0.058	0.051	0.039	0.027
		77/04	301	0.039	0.037	0.033	0.028	0.022
		77/05	282	0.036	0.035	0.031	0.026	0.022
5	Albq.	77/06	159	0.054	0.053	0.050	0.042	0.031
		77/07	303	0.041	0.040	0.036	0.031	0.024
		77/09	234	0.039	0.039	0.036	0.031	0.027
		77/10	239	0.041	0.040	0.039	0.037	0.032
		77/11	221	0.058	0.057	0.054	0.048	0.034
		77/12	202	0.053	0.052	0.049	0.042	0.036
6	Ft. Hood	76/07	131	0.040	0.039	0.037	0.035	0.027
		76/08	361	0.034	0.033	0.031	0.026	0.022
		76/09	121	0.041	0.040	0.036	0.036	0.029
		76/10	115	0.050	0.049	0.047	0.041	0.033
		76/11	88	0.027	0.026	0.025	0.024	0.011
		76/11	84	0.035	0.032	0.026	0.021	0.016
		76/12	155	0.053	0.051	0.044	0.036	0.027

SERI ◉

Table 4-3. MONTHLY AVERAGE CIRCUMSOLAR RATIO $R_{av}(q)$ VERSUS THRESHOLD q FOR EACH FILE (concluded)

File	Location	Yr/Mo	Hours of Data	q (W/m^2) 0	50	150	300	500
7	Ft. Hood	77/01	155	0.062	0.061	0.058	0.047	0.037
		77/02	165	0.053	0.052	0.049	0.042	0.031
		77/03	248	0.084	0.081	0.075	0.063	0.049
		77/04	101	0.027	0.027	0.026	0.024	0.021
8	Ft. Hood	77/07	74	0.040	0.038	0.037	0.036	0.031
	Argonne	77/08	63	0.124	0.120	0.098	0.078	0.063
		77/09	140	0.095	0.091	0.085	0.076	0.055
		77/10	152	0.079	0.069	0.062	0.055	0.046
		77/11	130	0.094	0.083	0.073	0.067	0.043
		77/12	115	0.148	0.127	0.112	0.100	0.078
9	China Lake	76/07	187	0.031	0.030	0.027	0.025	0.017
		76/08	392	0.013	0.013	0.012	0.011	0.009
		76/09	35	0.030	0.030	0.026	0.022	0.020
		76/10	262	0.023	0.023	0.021	0.019	0.016
		76/11	246	0.025	0.024	0.023	0.020	0.016
		76/12	268	0.026	0.026	0.025	0.023	0.016
10	China Lake	77/01	176	0.044	0.043	0.038	0.036	0.025
		77/02	248	0.045	0.044	0.043	0.036	0.027
		77/03	143	0.052	0.052	0.051	0.043	0.037
11	Barstow	77/07	33	0.083	0.082	0.080	0.077	0.064
		77/08	341	0.030	0.029	0.027	0.024	0.019
		77/09	265	0.028	0.028	0.026	0.023	0.020
		77/10	232	0.042	0.041	0.040	0.034	0.027
		77/11	268	0.061	0.059	0.056	0.047	0.033
		77/12	236	0.058	0.054	0.050	0.039	0.025
12	Barstow	78/01	59	0.080	0.074	0.064	0.060	0.039
		78/02	65	0.061	0.058	0.054	0.041	0.029
		78/03	136	0.030	0.028	0.025	0.017	0.014
		78/04	284	0.042	0.040	0.039	0.033	0.022
		78/05	411	0.034	0.034	0.032	0.028	0.025
		78/06	247	0.024	0.024	0.023	0.022	0.020

SERI❂

SERI ✲ ──────────────────────────────────

SECTION 5.0

MEASUREMENTS OF SOLAR RADIATION

The LBL data map out the solar brightness up to an angle $\Delta = 3.2°$. This somewhat arbitrary cutoff was chosen in order to permit sufficiently accurate calculation of the radiation measured by a normal incidence pyrheliometer (NIP). To appreciate this detail one must recognize that the NIP does not have a sharp cutoff at 2.75° but is characterized by the angular acceptance function in Fig. 5-1.* For angles below 3.2°, f_{NIP} is given by

$$f_{NIP}(\theta) = \begin{cases} 1 & \text{for } \theta < 0.02793 \text{ rad (or } 1.6°) \\ 1.714 - 25.55\,\theta & \text{for } 0.02793 \text{ rad} < \theta < 0.05585 \text{ rad} \ . \end{cases} \qquad (5\text{-}1)$$

Because almost all available measurements of so-called direct or beam irradiance I_b have been obtained with a NIP and because this will also be the case in the foreseeable future, it is desirable to refer the intercept factor to I_b. On the other hand, we have followed the LBL group in defining the circumsolar component I_c as the total irradiance between 0.275° and 3.2°. This inclusion in I_c of all radiation out to 3.2° is motivated by the desire to calculate the insolation available to focusing collectors as accurately as the data permit (some focusing collectors do intercept some appreciable radiation that the pyrheliometer misses).

As a consequence of these definitions, I_b is somewhat smaller than the irradiance $I_s + I_c$ on which all intercept factors calculated so far have been based. The difference between I_b and $I_s + I_c$ is small on clear days but increases with circumsolar ratio.

We want to reconcile the above definition of circumsolar radiation with the goal of providing a single expression for an intercept factor γ that is based on I_b so that I_{in} can be obtained from

$$I_{in} = \gamma\, I_b \ . \qquad (5\text{-}2)$$

The NIP behaves optically like a solar collector with angular acceptance function $f_{NIP}(\theta)$; hence, the irradiance measured by a NIP is

$$I_b = \gamma_{NIP}(I_s + I_c) \ , \qquad (5\text{-}3)$$

─────────────────────

*Information given by D. F. Grether in a telephone conversation.

SERI
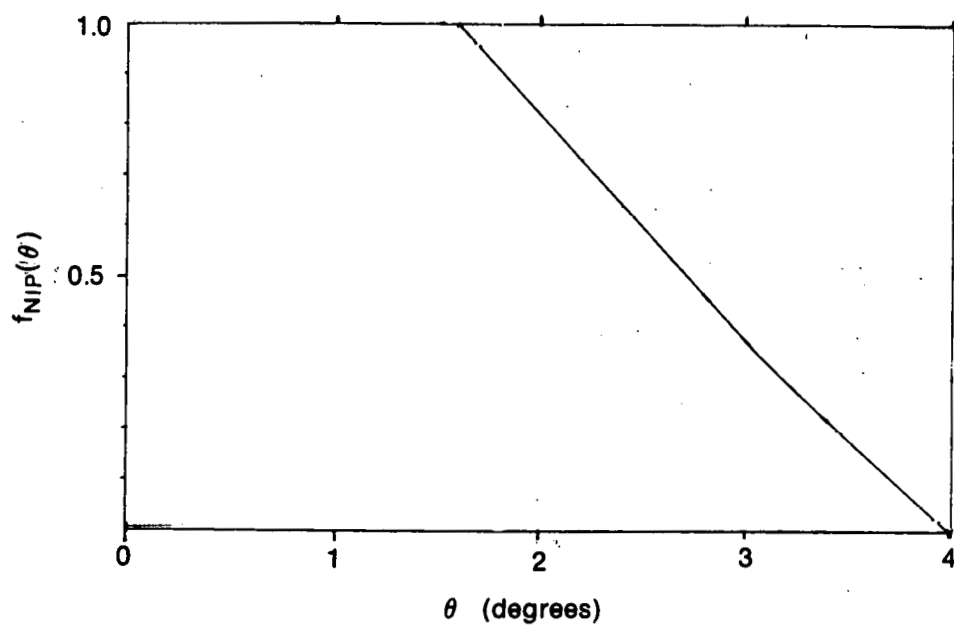
Figure 5-1. Angular Acceptance Function of Pyrheliometer (NIP)

where

$$\gamma_{NIP} = \frac{2\pi}{\overline{I}_s + \overline{I}_c} \int_0^\Delta \theta \, B(\theta) \, f_{NIP}(\theta) \, d\theta \quad . \tag{5-4}$$

For the purpose of calculating long-term average intercept factors the standard scan (Table 4-1) can be used in Eq. 5-4 with the result

$$\gamma_{NIP,av} = 1 - 0.09632 \, R_{av} \quad . \tag{5-5}$$

Now the intercept factor $\gamma_{sc,av}$ of Eq. 4-12, which was based on $\overline{I}_s + \overline{I}_c$, can be related to the beam irradiance $\overline{I}_b$. Equation 4-11 can be rewritten as

$$\overline{I}_{in} = \gamma_{sc,av} \, (\overline{I}_s + \overline{I}_c) \quad .$$

Replacing $\overline{I}_s + \overline{I}_c$ with $\overline{I}_b / \gamma_{NIP,av}$ from Eq. 5-3 yields

$$\overline{I}_{in} = \frac{\gamma_{sc,av}}{\gamma_{NIP,av}} \, \overline{I}_b \quad . \tag{5-6}$$

Finally, Eqs. 4-12 and 5-5 are inserted to display the dependence on circum-solar ratio R_{av}

$$\overline{I}_{in} = \frac{\gamma_{s,av} - \left(\gamma_{s,av} - \gamma_{c,av}\right) R_{av}}{1 - 0.09632 \, R_{av}} \, \overline{I}_b \quad . \tag{5-7}$$

SERI⊕

SECTION 6.0

NUMERICAL RESULTS AND VALIDATION

To validate the linear model (Eq. 4-12), a wide range of parabolic dish collectors were considered, with concentration ratios C = 200, 500, 1000, 2000, 5000, and 10,000; rim angles ϕ = 30°, 40°, 50°, and 60°; optical errors ranging from σ = 1 mrad to 30 mrad; and four operating thresholds q = 50, 150, 300, and 500 W/m^2. The validation is typical of other focusing collectors as well, because any practical solar concentrator of concentration sufficiently high to be susceptible to circumsolar radiation has an angular acceptance function $f(\theta)$ with the same general behavior as a parabolic dish: $f(\theta)$ is constant out to an angle θ, and then decreases smoothly to zero at θ_2. The above range of C and ϕ values covers all typical cases.

For each collector design (i.e., for each value of ϕ, C, and σ) and for each scan $B_i(\theta)$ in the LBL data set,* the intercept factor $\gamma_{sc,i}$ was calculated exactly; i.e., according to Eq. 3-5. Then the exact long-term average intercept factor for each file was calculated as

$$\gamma_{sc,av,exact} = \frac{\sum_{i+} \gamma_{sc,i,exact} (I_s + I_c)_i}{\sum_{i+} (I_s + I_c)_i} , \qquad (6-1)$$

the summation running over all scans in the file. With 120 collector designs, 4 threshold values, and 12 files, this required 4 × 120 × 12 = 5760 hour-by-hour simulations. Then $\gamma_{sc,av,model}$ for the linear model, Eq. 4-12, was calculated for each collector design and for each file of circumsolar data, and the error

$$\varepsilon = \gamma_{sc,av,model} - \gamma_{sc,av,exact} \qquad (6-2)$$

was determined. To list ε for each of the almost 6000 simulations may be more confusing than informative; hence, the results for several simulations were grouped together and the mean and the rms errors were calculated for each category.

Let ε_{cqf} designate the error (Eq. 6-2) for collector design c, threshold q, and file f. For each collector design c (i.e., for each value of C, ϕ, and σ), the mean error or bias was calculated as

---

*The original LBL data were measured in 10-minute intervals. The data supplied to us were hourly averages of the original measurements.

$$\bar{\varepsilon}_c = \frac{1}{12} \sum_{f=1}^{12} \frac{1}{4} \sum_{q=1}^{4} \varepsilon_{cqf} \qquad (6\text{-}3)$$

and the rms error as

$$\bar{\varepsilon}_{c,rms} = \left(\frac{1}{12} \sum_{f=1}^{12} \frac{1}{4} \sum_{q=1}^{4} \varepsilon_{cqf}^2 \right)^{1/2} . \qquad (6\text{-}4)$$

The results are listed in Table 6-1, together with the values for $\gamma_{s,av}$ and $(\gamma_{s,av} - \gamma_{c,av})$ of the linear model for the long-term average intercept factor.

To evaluate possible location- or threshold-dependent trends, the mean and rms error for each file and threshold also have been calculated but averaged over all collector designs:

$$\bar{\varepsilon}_{qf} = \frac{1}{120} \sum_{c=1}^{120} \varepsilon_{cqf} \qquad (6\text{-}5)$$

and

$$\bar{\varepsilon}_{qf,rms} = \left(\frac{1}{120} \sum_{c=1}^{120} \varepsilon_{cqf}^2 \right)^{1/2} . \qquad (6\text{-}6)$$

These results, listed in Table 6-2, show that there is no significant pattern with regard to threshold or location.

The single most important measure of the error is provided by the average over all collector designs, thresholds, and files. The results for the bias error and for the rms error are

$$\bar{\varepsilon}_{total} = \frac{1}{5760} \sum_{c=1}^{120} \sum_{q=1}^{4} \sum_{f=1}^{12} \varepsilon_{cqf} = 0.00056 \qquad (6\text{-}7)$$

and

$$\bar{\varepsilon}_{total,rms} = \left(\frac{1}{5760} \sum_{c=1}^{120} \sum_{q=1}^{4} \sum_{f=1}^{12} \varepsilon_{cqf} \right)^{1/2} = 0.0021 . \qquad (6\text{-}8)$$

Table 6-1. VALIDATION OF LINEAR MODEL FOR INTERCEPT FACTOR FOR PARABOLIC DISH OF RIM ANGLE φ, CONCENTRATION C, AND OPTICAL ERROR σ

φ	C	σ (mrad)	$\gamma_{s,av}$	$\gamma_{s,av} - \gamma_{c,av}$	$\bar{\epsilon}$	$\bar{\epsilon}_{rms}$
30.	200.	14.0	0.9539	0.2467	-0.0001	0.0008
30.	200.	18.0	0.8489	0.2175	-0.0001	0.0006
30.	200.	22.0	0.7206	0.1715	-0.0000	0.0005
30.	200.	26.0	0.6000	0.1283	+0.0000	0.0004
30.	200.	30.0	0.4984	0.0943	+0.0000	0.0003
30.	500.	10.0	0.9067	0.3858	-0.0002	0.0008
30.	500.	12.0	0.8126	0.3377	-0.0002	0.0007
30.	500.	14.0	0.7115	0.2827	-0.0001	0.0006
30.	500.	16.0	0.6163	0.2310	-0.0001	0.0005
30.	500.	18.0	0.5325	0.1867	+0.0000	0.0004
30.	1000.	6.0	0.9531	0.5184	-0.0005	0.0009
30.	1000.	7.0	0.9017	0.4910	-0.0005	0.0009
30.	1000.	8.0	0.8372	0.4511	-0.0004	0.0008
30.	1000.	9.0	0.7668	0.4053	-0.0004	0.0007
30.	1000.	10.0	0.6966	0.3590	-0.0003	0.0006
30.	2000.	3.0	0.9914	0.6444	-0.0008	0.0011
30.	2000.	4.0	0.9525	0.6294	-0.0009	0.0013
30.	2000.	5.0	0.8786	0.5794	-0.0008	0.0015
30.	2000.	6.0	0.7850	0.5087	-0.0007	0.0014
30.	2000.	7.0	0.6882	0.4339	-0.0005	0.0012
30.	5000.	1.5	0.9874	0.8029	-0.0016	0.0020
30.	5000.	2.0	0.9560	0.7807	-0.0016	0.0029
30.	5000.	2.5	0.9060	0.7380	-0.0016	0.0038
30.	5000.	3.0	0.8431	0.6812	-0.0015	0.0039
30.	5000.	3.5	0.7737	0.6171	-0.0013	0.0037
30.	10000.	1.0	0.9275	0.8722	-0.0024	0.0070
30.	10000.	1.5	0.8515	0.7883	-0.0022	0.0082
30.	10000.	2.0	0.7670	0.6979	-0.0019	0.0077
30.	10000.	2.5	0.6810	0.6078	-0.0014	0.0066
30.	10000.	3.0	0.5982	0.5224	-0.0010	0.0052
40.	200.	14.0	0.9913	0.1530	-0.0000	0.0008
40.	200.	18.0	0.9499	0.1640	-0.0000	0.0006
40.	200.	22.0	0.8711	0.1537	-0.0000	0.0005
40.	200.	26.0	0.7735	0.1312	+0.0000	0.0004
40.	200.	30.0	0.6752	0.1062	+0.0000	0.0003
40.	500.	10.0	0.9757	0.3228	-0.0002	0.0009
40.	500.	12.0	0.9305	0.3124	-0.0002	0.0008
40.	500.	14.0	0.8645	0.2869	-0.0001	0.0007
40.	500.	16.0	0.7879	0.2532	-0.0001	0.0005
40.	500.	18.0	0.7095	0.2177	-0.0000	0.0005
40.	1000.	6.0	0.9911	0.4422	-0.0004	0.0010
40.	1000.	7.0	0.9738	0.4424	-0.0004	0.0010
40.	1000.	8.0	0.9440	0.4329	-0.0004	0.0009
40.	1000.	9.0	0.9028	0.4139	-0.0003	0.0008
40.	1000.	10.0	0.8535	0.3878	-0.0003	0.0007
40.	2000.	3.0	0.9992	0.5503	-0.0007	0.0012
40.	2000.	4.0	0.9912	0.5594	-0.0007	0.0012

Table 6-1. VALIDATION OF LINEAR MODEL FOR INTERCEPT FACTOR FOR PARABOLIC DISH OF RIM ANGLE ϕ, CONCENTRATION C, AND OPTICAL ERROR σ (continued)

ϕ	C	σ (mrad)	$\gamma_{s,av}$	$\gamma_{s,av} - \gamma_{c,av}$	$\bar{\epsilon}$	$\bar{\epsilon}_{rms}$
40.	2000.	5.0	0.9644	0.5540	-0.0007	0.0013
40.	2000.	6.0	0.9145	0.5277	-0.0006	0.0012
40.	2000.	7.0	0.8472	0.4847	-0.0005	0.0011
40.	5000.	1.5	0.9991	0.7108	-0.0013	0.0017
40.	5000.	2.0	0.9934	0.7152	-0.0013	0.0023
40.	5000.	2.5	0.9779	0.7108	-0.0014	0.0029
40.	5000.	3.0	0.9497	0.6938	-0.0013	0.0031
40.	5000.	3.5	0.9094	0.6641	-0.0012	0.0031
40.	10000.	1.0	0.9909	0.8395	-0.0021	0.0052
40.	10000.	1.5	0.9627	0.8185	-0.0020	0.0062
40.	10000.	2.0	0.9132	0.7740	-0.0018	0.0063
40.	10000.	2.5	0.8487	0.7131	-0.0015	0.0058
40.	10000.	3.0	0.7762	0.6437	-0.0012	0.0049
50.	200.	14.0	0.9961	0.0931	-0.0000	0.0007
50.	200.	18.0	0.9761	0.1114	-0.0000	0.0005
50.	200.	22.0	0.9300	0.1178	-0.0000	0.0005
50.	200.	26.0	0.8616	0.1121	+0.0000	0.0004
50.	200.	30.0	0.7817	0.0992	+0.0000	0.0003
50.	500.	10.0	0.9890	0.2565	-0.0001	0.0009
50.	500.	12.0	0.9656	0.2587	-0.0001	0.0008
50.	500.	14.0	0.9258	0.2510	-0.0001	0.0007
50.	500.	16.0	0.8724	0.2345	-0.0001	0.0006
50.	500.	18.0	0.8107	0.2126	-0.0000	0.0005
50.	1000.	6.0	0.9961	0.3779	-0.0003	0.0011
50.	1000.	7.0	0.9881	0.3823	-0.0003	0.0010
50.	1000.	8.0	0.9730	0.3823	-0.0003	0.0009
50.	1000.	9.0	0.9497	0.3765	-0.0003	0.0008
50.	1000.	10.0	0.9186	0.3647	-0.0003	0.0007
50.	2000.	3.0	0.9996	0.4888	-0.0006	0.0012
50.	2000.	4.0	0.9961	0.4973	-0.0006	0.0012
50.	2000.	5.0	0.9836	0.5009	-0.0006	0.0012
50.	2000.	6.0	0.9567	0.4935	-0.0006	0.0011
50.	2000.	7.0	0.9145	0.4731	-0.0005	0.0010
50.	5000.	1.5	0.9995	0.6477	-0.0011	0.0016
50.	5000.	2.0	0.9971	0.6526	-0.0012	0.0020
50.	5000.	2.5	0.9902	0.6548	-0.0012	0.0024
50.	5000.	3.0	0.9764	0.6512	-0.0012	0.0026
50.	5000.	3.5	0.9542	0.6399	-0.0011	0.0026
50.	10000.	1.0	0.9959	0.7762	-0.0018	0.0043
50.	10000.	1.5	0.9836	0.7719	-0.0018	0.0052
50.	10000.	2.0	0.9581	0.7551	-0.0017	0.0053
50.	10000.	2.5	0.9181	0.7233	-0.0015	0.0050
50.	10000.	3.0	0.8659	0.6786	-0.0013	0.0044
60.	200.	14.0	0.9945	0.0732	-0.0000	0.0006
60.	200.	18.0	0.9757	0.0859	-0.0000	0.0005
60.	200.	22.0	0.9394	0.0921	+0.0000	0.0005

SERI

Table 6-1. VALIDATION OF LINEAR MODEL FOR INTERCEPT FACTOR FOR PARABOLIC DISH OF RIM ANGLE φ, CONCENTRATION C, AND OPTICAL ERROR σ (concluded)

φ	C	σ (mrad)	$\gamma_{s,av}$	$\gamma_{s,av} - \gamma_{c,av}$	$\bar{\epsilon}$	$\bar{\epsilon}_{rms}$
60.	200.	26.0	0.8869	0.0913	+0.0000	0.0004
60.	200.	30.0	0.8234	0.0850	+0.0000	0.0003
60.	500.	10.0	0.9871	0.2132	-0.0001	0.0009
60.	500.	12.0	0.9671	0.2154	-0.0001	0.0008
60.	500.	14.0	0.9361	0.2119	-0.0001	0.0007
60.	500.	16.0	0.8952	0.2030	-0.0001	0.0006
60.	500.	18.0	0.8469	0.1896	-0.0000	0.0005
60.	1000.	6.0	0.9944	0.3386	-0.0003	0.0011
60.	1000.	7.0	0.9863	0.3409	-0.0003	0.0010
60.	1000.	8.0	0.9731	0.3402	-0.0003	0.0009
60.	1000.	9.0	0.9545	0.3360	-0.0003	0.0009
60.	1000.	10.0	0.9306	0.3283	-0.0002	0.0008
60.	2000.	3.0	0.9991	0.4544	-0.0005	0.0012
60.	2000.	4.0	0.9944	0.4599	-0.0005	0.0012
60.	2000.	5.0	0.9821	0.4608	-0.0005	0.0012
60.	2000.	6.0	0.9599	0.4547	-0.0005	0.0011
60.	2000.	7.0	0.9275	0.4407	-0.0005	0.0010
60.	5000.	1.5	0.9988	0.6130	-0.0010	0.0015
60.	5000.	2.0	0.9952	0.6153	-0.0010	0.0018
60.	5000.	2.5	0.9878	0.6151	-0.0011	0.0022
60.	5000.	3.0	0.9755	0.6111	-0.0011	0.0023
60.	5000.	3.5	0.9577	0.6025	-0.0010	0.0023
60.	10000.	1.0	0.9925	0.7355	-0.0017	0.0038
60.	10000.	1.5	0.9802	0.7291	-0.0017	0.0046
60.	10000.	2.0	0.9597	0.7159	-0.0016	0.0047
60.	10000.	2.5	0.9298	0.6940	-0.0014	0.0045
60.	10000.	3.0	0.8905	0.6629	-0.0013	0.0040

Table 6-2. BIAS $\bar{\epsilon}$ AND rms ERROR $\bar{\epsilon}_{rms}$ AVERAGED OVER COLLECTOR DESIGNS, FOR DIFFERENT LOCATIONS WITH THRESHOLD q AND CIRCUMSOLAR RATIO R_{av}.

File	q (W/m^2)	R_{av}	$\bar{\epsilon}$	$\bar{\epsilon}_{rms}$
1	50	0.059	-0.0015	0.0030
1	150	0.050	-0.0016	0.0030
1	300	0.038	-0.0015	0.0029
1	500	0.024	-0.0015	0.0024
2	50	0.052	-0.0015	0.0022
2	150	0.046	-0.0017	0.0024
2	300	0.036	-0.0013	0.0019
2	500	0.026	-0.0016	0.0022
3	50	0.031	-0.0001	0.0002
3	150	0.028	-0.0002	0.0004
3	300	0.024	-0.0003	0.0005
3	500	0.019	-0.0001	0.0004
4	50	0.039	-0.0002	0.0013
4	150	0.035	-0.0001	0.0013
4	300	0.029	+0.0003	0.0014
4	500	0.022	+0.0006	0.0016
5	50	0.046	-0.0008	0.0010
5	150	0.043	-0.0010	0.0011
5	300	0.038	-0.0011	0.0013
5	500	0.030	-0.0008	0.0010
6	50	0.039	+0.0002	0.0029
6	150	0.036	-0.0001	0.0029
6	300	0.031	-0.0002	0.0029
6	500	0.024	-0.0008	0.0030
7	50	0.059	-0.0004	0.0019
7	150	0.055	-0.0011	0.0026
7	300	0.047	-0.0008	0.0025
7	500	0.036	-0.0010	0.0023
8	50	0.073	-0.0017	0.0033
8	150	0.065	-0.0017	0.0033
8	300	0.058	-0.0020	0.0036
8	500	0.044	-0.0024	0.0039
9	50	0.022	+0.0009	0.0015
9	150	0.020	+0.0008	0.0015
9	300	0.018	+0.0006	0.0013
9	500	0.014	+0.0007	0.0014
10	50	0.046	-0.0002	0.0027
10	150	0.044	-0.0004	0.0023
10	300	0.038	-0.0006	0.0024
10	500	0.029	-0.0001	0.0024
11	50	0.042	-0.0001	0.0012
11	150	0.039	-0.0004	0.0010
11	300	0.033	-0.0006	0.0012
11	500	0.025	-0.0001	0.0011
12	50	0.035	+0.0002	0.0005
12	150	0.033	-0.0000	0.0003
12	300	0.028	-0.0001	0.0004
12	500	0.023	+0.0000	0.0004

To put the results for the average errors into perspective, note that the circumsolar ratio varies considerably from year to year. For example, for the same month and for the same location (June, Albuquerque, N. Mex.), R_{av} for $q = 50$ W/m^2 is 0.028 in 1976 and 0.053 in 1977, as shown by Table 4-3. Since the coefficient $(\gamma_{s,av} - \gamma_{c,av})$ of the circumsolar correction term for the average intercept factor is on the order of 0.5, the inherent error of the linear model is much smaller than the error introduced by uncertainties in the circumsolar ratio (unless the average circumsolar ratio is known to better than 0.004 absolute error, which is unlikely to be the case in the near future). Furthermore, an error of a fraction of a percent in an intercept factor is very small compared to the uncertainty in the long-term average values of reflectance and absorptance. Therefore, the linear model for the average intercept factor is satisfactory unless circumsolar ratios and material properties are known within a small fraction of a percent.

An interesting result from Table 6-1 concerns the rim angle dependence of the intercept factor. For a given C and σ, the coefficients $\gamma_{s,av}$ and $\gamma_{c,av}$ can vary considerably with rim angle; e.g., for C = 500 and $\sigma = 10$ mrad, the coefficient $(\gamma_{s,av} - \gamma_{c,av})$ is 0.386 for $\phi = 30°$ and 0.213 for $\phi = 60°$. This implies that the collector with a 30° rim angle is nearly twice as sensitive to circumsolar radiation as the collector with a 60° rim angle. Therefore, an optical model with sharp angular cutoff, as assumed by Biggs and Vittitoe (1979) and Grether et al. (1977d), may not be sufficiently accurate for calculating the effect of circumsolar radiation.

For other concentrator types, e.g., Fresnel lenses and central receivers, the intercept factors $\gamma_{s,av}$ and $\gamma_{c,av}$ can be calculated in a similar manner. Specific results for the important case of a parabolic trough with 90° rim angle and cylindrical receiver are shown in Table 6-3 for a range of concentration C and optical error σ, at normal incidence. It is instructive to compare these results with the ones for point focus parabolas. Whereas for point focus parabolas (Table 6-1) the value of $(\gamma_{s,av} - \gamma_{c,av})$ ranges from 0.1 to 0.8, values for the line focus parabolas are much smaller, in the range of 0.03 to 0.4. Since the sensitivity to circumsolar radiation is proportional to $(\gamma_{s,av} - \gamma_{c,av})$, the line focus parabolas tend to be significantly less sensitive to circumsolar radiation than point focus parabolas. [At nonnormal incidence the effect of circumsolar radiation on line focus collectors may be enhanced, however, because of an increase in the projected width of the sun (Bendt et al. 1979).] This difference is easy to understand in terms of the rms angular width of the sun which is a factor $\sqrt{2}$ larger for point focus geometry than for line focus geometry.

Table 6-3. THE INTERCEPT FACTORS $\gamma_{s,av}$ and ($\gamma_{s,av}$ - $\gamma_{c,av}$) FOR PARABOLIC TROUGH WITH 90° RIM ANGLE, CYLINDRICAL RECEIVER, GEOMETRIC CONCENTRATION C, AND TOTAL OPTICAL ERROR σ

C	σ (mrad)	$\gamma_{s,av}$	$\gamma_{s,av}$ - $\gamma_{c,av}$
10.	3.0	1.0000	.0262
10.	4.0	1.0000	.0269
10.	5.0	1.0000	.0279
10.	6.0	1.0000	.0292
10.	8.0	1.0000	.0324
10.	10.0	.9999	.0366
10.	15.0	.9946	.0490
10.	20.0	.9733	.0568
15.	3.0	1.0000	.1031
15.	4.0	1.0000	.1045
15.	5.0	1.0000	.1064
15.	6.0	.9996	.1089
15.	8.0	.9989	.1149
15.	10.0	.9941	.1205
15.	15.0	.9549	.1221
15.	20.0	.8830	.1068
20.	3.0	1.0000	.1787
20.	4.0	1.0000	.1812
20.	5.0	.9997	.1845
20.	6.0	.9986	.1880
20.	8.0	.9905	.1929
20.	10.0	.9712	.1916
20.	15.0	.8815	.1626
20.	20.0	.7714	.1219
25.	3.0	1.0000	.2432
25.	4.0	.9996	.2471
25.	5.0	.9976	.2510
25.	6.0	.9926	.2534
25.	8.0	.9696	.2501
25.	10.0	.9302	.2354
25.	15.0	.7972	.1750
25.	20.0	.6701	.1199
30.	3.0	.9998	.2990
30.	4.0	.9977	.3034
30.	5.0	.9914	.3056
30.	6.0	.9793	.3037
30.	8.0	.9369	.2866
30.	10.0	.8775	.2565
30.	15.0	.7167	.1731
30.	20.0	.5861	.1121
40.	3.0	.9960	.3903
40.	4.0	.9844	.3892
40.	5.0	.9625	.3799
40.	6.0	.9311	.3627
40.	8.0	.8504	.3132
40.	10.0	.7641	.2595
40.	15.0	.5841	.1551
40.	20.0	.4625	.0945

SECTION 7.0

SUMMARY AND CONCLUSIONS

Starting with a review of the circumsolar results provided by Lawrence Berkeley Laboratory (LBL) and with a description of the optical analysis of focusing collectors, we derived a simple prescription for incorporating circumsolar effects into any analysis of solar energy systems. Both the effect on instantaneous performance (of interest for collector testing and for detailed system simulations) and the effect on long-term average performance (expressed as a correction term for calculations that did not take circumsolar radiation into account) have been treated. The formulas presented are at least as accurate as any circumsolar data that will be available in the foreseeable future. The results also suggest priorities for further acquisition and analysis of circumsolar data.

7.1 INSTANTANEOUS PERFORMANCE

If the greatest possible accuracy in a system simulation is desired and if circumsolar data of the LBL type are available, Eq. 3-5 should be used for computing the collector performance for each circumsolar scan. For this purpose one first calculates the smeared angular acceptance function $f_\sigma(\theta)$ for the concentrator in question. The function $f_\sigma(\theta)$ depends only on the optics but not on insolation; its calculation is described in Section 3.0. Then $f_\sigma(\theta)\ \theta\Delta\theta$ is stored in memory at the beginning of the simulation; this involves 56 numbers, one for each of the angles at which the brightness has been measured by LBL ($\Delta\theta$ is the increment between these angles). The intercepted irradiance I_{in} for each scan is then computed according to the discrete version of Eq. 3-5:*

$$I_{in} = 2\pi \sum_{i=1}^{56} B(\theta_i)\ f_\sigma(\theta_i)\ \theta_i \Delta\theta_i \ , \tag{7-1}$$

with $B(\theta_i)$ as the brightness of the scan at angle θ_i. Equation 7-1 requires 56 multiplications and additions, certainly not an excessive computational effort.

As for collector testing, the first step is to decide whether circumsolar radiation can have any detectable effect at all. For this purpose one calculates the coefficients $\gamma_{s,av}$ and $\gamma_{c,av}$ of the long-term average model (Eqs. 7-2

---

*Even though Eq. 7-1 has been derived for point focus geometry, it can also be used for line focus concentrations if the line focus angular acceptance function is transformed to the equivalent point focus angular acceptance function according to Eq. 3-8.

to 7-5). To ensure standardized test results, collectors should be tested only on very clear days. Since on clear days the circumsolar ratio ranges from less than 1 percent to, at most, a few percent, it follows that a collector test will be sensitive to circumsolar effects only if variations in the intercept factor on the order of $\Delta R(\gamma_{s,av} - \gamma_{c,av})$ with $\Delta R \approx 0.01$ can be measured. If this is the case and if one wants to guarantee that the analysis is as accurate as possible, the brightness distribution of the sun should be monitored during the test with a circumsolar telescope of the LBL type. The intercepted radiation is then calculated according to Eq. 7-1. For example, Table 6-1 shows that parabolic dish collectors with a 45° rim angle and concentration below 1000 have $(\gamma_{s,av} - \gamma_{c,av})$ values below 0.5. If the experimental error in the optical efficiency

$$\eta_o = (\rho\tau\alpha)\ \gamma \qquad (7\text{-}2)$$

is greater than 0.5 $\Delta R \approx 0.005$, circumsolar radiation will have no detectable effect on tests of such collectors on clear days.

7.2 LONG-TERM AVERAGE PERFORMANCE

The simplest way to account for circumsolar effects on long-term average performance is to start with the usual pyrheliometer data for the beam irradiance I_b and to calculate the intercepted irradiance

$$I_{in} = \gamma_{av} I_b \quad ,$$

with the intercept factor

$$\gamma_{av} = \frac{\gamma_{s,av} - (\gamma_{s,av} - \gamma_{c,av})\ R_{av}(q)}{1 - 0.0963\ R_{av}(q)} \quad . \qquad (7\text{-}3)$$

$R_{av}(q)$ is the long-term average circumsolar ratio (Eq. 4-13) for the location and period in question; to a good approximation it is a linear function of the threshold q.* For the locations where circumsolar data are available, $R_{av}(q)$ for $q = 50$ W/m^2 and 500 W/m^2 for each month has been calculated and listed in Table 4-3. The circumsolar ratio for any other threshold value q can be found by linear interpolation.

The denominator of Eq. 7-3 corrects for the fact that a pyrheliometer does not measure all the circumsolar radiation out to angles of 3.2° that has been included in the calculation of R_{av} (see Section 5.0 for details).

---

*In thermal collectors the threshold is the heat loss divided by the optical efficiency.

The coefficients $\gamma_{s,av}$ and $\gamma_{c,av}$ needed in Eq. 7-3 are the intercept factors for radiation from the solar disk and from the circumsolar region, respectively, as calculated for the standard scan. This standard scan is the simple average over all circumsolar scans measured by LBL and it can be used for any location. It is listed in Tables 4-1 for point focus and in Table 4-2 for line focus geometry. For point focus collectors, the coefficients $\gamma_{s,av}$ and $\gamma_{c,av}$ are calculated from these scans according to the discrete versions of Eqs. 4-14 and 4-15,

$$\gamma_{s,av} = \sum_{i=1}^{11} w_s(\theta_i)\, \overline{B}(\theta_i)\, f_\sigma(\theta_i) \tag{7-4}$$

and

$$\gamma_{c,av} = \sum_{i=12}^{56} w_c(\theta_i)\, \overline{B}(\theta_i)\, f_\sigma(\theta_i) \quad , \tag{7-5}$$

where

f_σ = smeared angular acceptance function (convolution of angular acceptance function f with Gaussian error distribution of width σ) (see Eq. 3-4);

$\overline{B}$ = brightness, from second column of Table 4-1;

w_s, w_c = weighting factors, for correct normalization, from third and fourth columns of Table 4-1;

these quantities are evaluated at angle θ_i, first column of Table 4-1.

The values for f_σ, $\overline{B}$, and w are determined for each of the 56 angles θ for which the LBL telescopes have provided data. For point focus geometry, the weighting factors have been calculated according to the formulas

$$w_s(\theta_i) = \frac{\theta_i \Delta\theta_i}{\displaystyle\sum_{k=1}^{11} \overline{B}(\theta_k)\, \theta_k \Delta\theta_k} \tag{7-6}$$

and

$$w_c(\theta_i) = \frac{\theta_i \Delta\theta_i}{\displaystyle\sum_{k=12}^{56} \overline{B}(\theta_k)\, \theta_k \Delta\theta_k} \quad . \tag{7-7}$$

For line focus geometry the angle θ is omitted in the numerator and denominator, and hence the weighting factors for line focus collectors are constants, independent of θ_1, if Table 4-2 with its equal angular increments is used for the standard circumsolar scan:

$$w_{s,line} = \frac{1}{\displaystyle\sum_{i=1}^{11} \overline{B}_{line}(\theta_i)} = \frac{1}{784{,}201 \text{ W/m}^2 \text{ rad}} \qquad (7\text{-}8)$$

and

$$w_{c,line} = \frac{1}{\displaystyle\sum_{i=1}^{125} \overline{B}_{line}(\theta_i)} = \frac{1}{29{,}379 \text{ W/m}^2 \text{ rad}} \qquad (7\text{-}9)$$

Hence, the intercept factors for line focus geometry can be calculated most easily from the equations

$$\gamma_{s,av,line} = w_{s,line} \sum_{i=1}^{11} \overline{B}_{line}(\theta_i)\, f_\sigma(\theta_i) \qquad (7\text{-}10)$$

and

$$\gamma_{c,av,line} = w_{c,line} \sum_{i=1}^{125} \overline{B}_{line}(\theta_i)\, f_\sigma(\theta_i) \quad . \qquad (7\text{-}11)$$

An example illustrates the use of this formalism. Table 6-1 lists some typical parabolic dishes with their relevant optical parameters. For each collector, $\gamma_{s,av}$ and $(\gamma_{s,av} - \gamma_{c,av})$ have been calculated according to Eqs. 7-4 and 7-5. A parabolic dish with concentration C = 1000, rim angle $\phi = 40°$, and total optical error with rms width $\sigma = 7$ mrad has the coefficients

$$\gamma_{s,av} = 0.9738$$

and

$$\gamma_{s,av} - \gamma_{c,av} = 0.4424 \quad .$$

Suppose the operating threshold is q = 100 W/m^2; the corresponding average circumsolar ratio is found by linear interpolation between the q = 50 W/m^2 and the q = 150 W/m^2 entries in Table 4-3. One of the lowest ratios in the table occurred in Albuquerque, N. Mex., in May 1976 with R_{av}(50 W/m^2) = 0.020 and R_{av}(150 W/m^2) = 0.019; hence, R_{av}(100 W/m^2) = 0.0195. The corresponding intercept factor is, from Eq. 7-3,

$$\gamma_{av} = \frac{0.9738 - (0.4424 \times 0.0195)}{1 - (0.0963 \times 0.0195)} = 0.967$$

with respect to the radiation I_h measured by a pyrheliometer. The highest average circumsolar ratio observed so far is that for Argonne, Ill., in August 1977. Interpolation yields $R_{av}(100 \text{ W/m}^2) = 0.120$, and the corresponding intercept factor is $\gamma_{av} = 0.931$, some 4% lower than that for Albuquerque in May 1976.

7.3 AVERAGE SUN SHAPE AND LIMB DARKENING

It is a well-known fact that the brightness of the solar disk as viewed from the earth is not uniform. Several investigators have recommended formulas to describe this so-called limb darkening (e.g., Biggs and Vittitoe 1979). These formulas, however, were based on rather limited measurements, and thus it was not clear to what extent they were really relevant for solar energy calculations. Our investigation has shown that a simple unweighted average over all circumsolar scans, when truncated at the solar radius $\delta = 0.275°$, is an excellent representation of limb darkening. (This value is slightly larger than the actual radius because of the limited angular resolution of the LBL data.) More precisely, when the intercept factor γ_s of point focus solar collectors for radiation from the solar disk is calculated for each scan in the LBL set and compared with the value $\gamma_{s,av}$ corresponding to the average sun shape, the rms error is at most 0.0002. We recommend, therefore, the average sun shape in Table 4-1 as the best choice for solar energy calculations in applications without spectral selectivity.

Similarly the analysis has shown that the average effect of circumsolar radiation can be calculated by means of a single standard brightness distribution in the circumsolar region; i.e., at angles between $\delta = 0.275°$ and $\Delta = 3.2°$. This distribution is also obtained from the average overall circumsolar profiles. The deviation of individual circumsolar scans from this shape is quite large; however, the average intercept factor $\gamma_{c,av}$ can still be calculated with an accuracy of ± 0.002.

As for the connection between solar and circumsolar shapes, the model introduces a discontinuity in the brightness distribution at the edge of the sun because the relative magnitudes of the solar and the circumsolar brightness profiles are allowed to vary with circumsolar ratio. This is not objectionable because it is carried out in a logically consistent manner. Also, at the edge of the sun the brightness of most scans drops very sharply by several orders of magnitude.

7.4 SPECTRAL EFFECTS

Because only spectrally averaged data were available, the numerical results of our analysis are applicable only to collectors without significant variation

of sensitivity within the solar spectrum. However, the formalism is independent of the spectrum, and the same analysis could and probably should be carried out for concentrators with photovoltaic receivers since the LBL telescope has also measured circumsolar data for separate portions of the solar spectrum.

7.5 NEED FOR FURTHER DATA OR CORRELATIONS

Circumsolar effects on focusing collectors are relatively small and, for practical applications, the effect on long-term average performance is of greatest interest. Therefore, a simple yet accurate correction procedure has been developed for predicting the average loss of performance due to circumsolar radiation. The model needs only one number as input: the average circumsolar ratio for the location and time period in question. As a single number, this average ratio (or quantities closely related to it) is much easier to measure and use than the detailed angular scans of the circumsolar telescope. For example, a modified pyrheliometer with variable field of view might be employed instead.

As an alternative to collecting actual data, one could attempt to correlate circumsolar ratios with beam irradiance and other quantities that might be relevant, such as air mass and diffuse irradiance. If reliable correlations of this type can be developed from the existing data base, then circumsolar effects at other locations can be predicted without additional data.

SECTION 8.0

REFERENCES

Bendt, P.; Rabl, A. 1979. Optical Analysis of Point Focus Parabolic Radiation Concentrators. Golden, CO: Solar Energy Research Institute; SERI/TR-34-336. Forthcoming.

Bendt, P.; Rabl, A.; Gaul, H. W.; Reed, K. A. 1979. Optical Analysis and Optimization of Line Focus Solar Collectors. Golden, CO: Solar Energy Research Institute; SERI/TR-34-092; September.

Biggs, F.; Vittitoe, C. N. 1979. The Helios Model for the Optical Behavior of Reflecting Solar Concentrators. Albuquerque, NM: Sandia Laboratories; SAND 76-0347.

Grether, D. F. 1979. Simplistic Maximum Scattering Model. Informal report.

Grether, D. F.; Hunt, A. 1977. Description of the LBL Reduced Data Base. Informal report. 9 August.

Grether, D. F.; Hunt, A.; Wahlig, M. 1977a. Techniques for Measuring Circumsolar Radiation. Berkeley, CA: Lawrence Berkeley Laboratory; LBL-8345.

Grether, D. F.; Hunt, A.; Wahlig, M. 1977b. Circumsolar Radiation: Correlations with Solar Radiation. Berkeley, CA: Lawrence Berkeley Laboratory; 11 October.

Grether, D. F.; Hunt, A.; Wahlig, M. 1977c. Circumsolar Radiation: Sensitivity Analysis for Central Receiver Designs. Berkeley, CA: Lawrence Berkeley Laboratory; 23 October.

Grether, D. F.; Hunt, A.; Wahlig, M. 1977d. Circumsolar Radiation: Monthly Summaries of Effect on Focussing Solar Energy Collection Systems. Berkeley, CA: Lawrence Berkeley Laboratory; 31 October.

Grether, D. F.; Evans, D.; Hunt, A.; Wahlig, M. 1979. "Application of Circumsolar Measurements to Concentrating Collectors." International Solar Energy Society Congress. 28 May - 1 June; Atlanta, GA.

Rabl, A. 1976. "Comparison of Solar Concentrators." Solar Energy. Vol. 18: p. 93.

Winston, R. 1970. "Light Collection Within the Framework of Geometrical Optics." J. Optical Society of America. Vol. 60: p. 245.

SERI🌐

Document Control Page	1. SERI Report No. TR-34-093	2. NTIS Accession No.	3. Recipient's Accession No.

4. Title and Subtitle	5. Publication Date
Effect of Circumsolar Radiation on Performance of Focusing Collectors	April 1980
	6.

7. Author(s)	8. Performing Organization Rept. No.
P. Bendt, A. Rabl	

9. Performing Organization Name and Address	10. Project/Task/Work Unit No. 3457.33
Solar Energy Research Institute 1617 Cole Boulevard Golden, Colorado 80401	11. Contract (C) or Grant (G) No. (C) (G)

12. Sponsoring Organization Name and Address	13. Type of Report & Period Covered Technical Report
	14.

15. Supplementary Notes

16. Abstract (Limit: 200 words) Circumsolar radiation is one of several factors, along with optical errors (contour, tracking, etc.), that determine the size and shape of the solar image at the receiver of a concentrating collector. The sensitivity of a collector to circumsolar radiation depends on insolation conditions and on collector parameters; it increases with geometrical concentration ratio and decreases with operating threshold. In this paper the Lawrence Berkeley Laboratory (LBL) circumsolar data are used to develop fast computational procedures for calculating the effect of circumsolar radiation on both the instantaneous and the long-term average performance of focusing collectors. For predictions of long-term average performance, a standard synthetic circumsolar scan has been developed that describes the brightness distribution of the solar disk ("limb darkening") and of the circumsolar region. The radiation intercepted by a receiver is calculated separately for the solar portion and for the circumsolar portion of this standard sun shape, and these two contributions are then weighted according to the long-term average circumsolar ratio for the location and period under study.

17. Document Analysis

a. Descriptors Circumsolar Radiation; Focusing Collectors; Insolation; Performance; Pyrheliometers; Optical properties; Mathematical Models; Circumsolar Scan

b. Identifiers/Open-Ended Terms

c. UC Categories

62

18. Availability Statement	19. No. of Pages
National Technical Information Service U. S. Department of Commerce 5285 Port Royal Road Springfield, Virginia 22161	65
	20. Price $5.25

Form No. 8200-13 (6-79)